Chapter 2

THEORETICAL BACKGROUND

This chapter discusses about theoretical background of medical imaging system overviews. Section 2.1 presents introduction and classification of different medical imaging modalities; Section 2.2 presents the fundamentals of transmission and emission tomography. Section 2.3 presents the basic concepts and mathematical background of various medical image reconstruction algorithms such as analytical, algebraic and statistical methods. Section 2.4 presents the literature survey of statistical iterative reconstruction (SIR) methods with their benefits and limitations. Section 2.5 presents the noise model for SIR methods. Section 2.6, presents the brief information about maximum a posteriori (MAP) estimation for statistical methods and their scope in this thesis. Section 2.7 presents the importance of regularization term in SIR methods. Section 2.8 presents the detailed discussion about various performance measures used for qualitative and quantitative analysis and finally the information about different datasets used in this thesis is stated in section 2.9.

2.1. Introduction

The field of medical imaging and image analysis has evolved due to the collective contributions from many areas of medicine, engineering, and basic sciences. The overall objective of medical imaging is to acquire useful information about the physiological processes or organs of the body by using external or internal sources of energy (X-Rays, Gamma Waves etc.) (A.P. Dhawan, 1990). Imaging

methods available today for radiological applications may use external, internal or a combination of energy sources (Fig. 1.2). In most commonly used imaging methods, ionized radiation such as X-rays is used as an external energy source primarily for anatomical imaging. Such anatomical imaging modalities are based on the attenuation coefficient of radiation passing through the body.

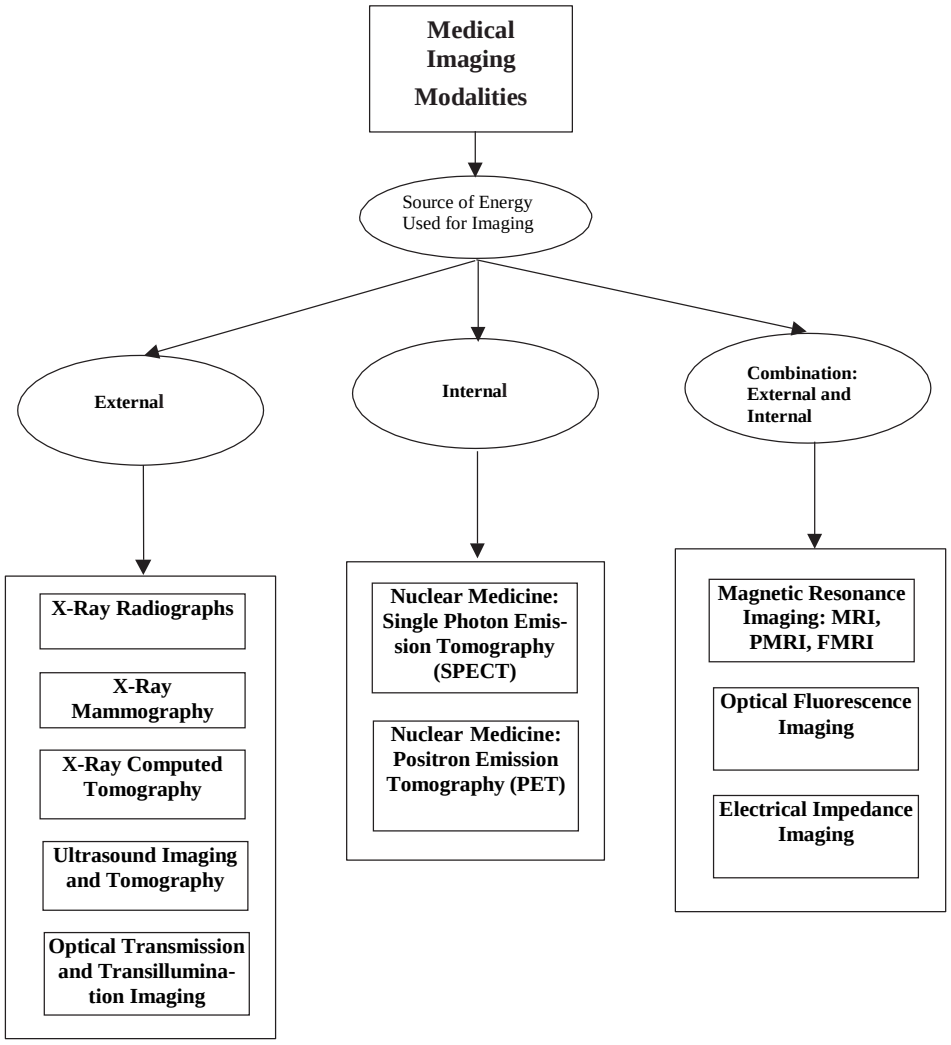

Fig. 2.1 A classification of different medical imaging modalities with respect to the type of energy source used for imaging (A.P. Dhawan, 2011).

For example, X-ray radiographs and X-ray CT imaging modalities measure attenuation coefficients of X ray that are based on the density of the tissue or part of the body being imaged. The images of chest radiographs show a spatial distribution of X-ray attenuation coefficients reflecting the overall density variations of the anatomical parts in the chest. Another example of external energy source-based imaging is ultrasound or acoustic imaging. Nuclear medi-

cine imaging modalities use an internal energy source through an emission process to image the human body. For emission imaging, radioactive pharmaceuticals are injected into the body to interact with selected body matter or tissue to form an internal source of radioactive energy that is used for imaging. The emission imaging principle is applied in SPECT and PET. Such types of nuclear medicine imaging modalities provide useful metabolic information about the physiological functions of the organs. Further, a clever combination of external stimulation on internal energy sources can be used in medical imaging to acquire more accurate information about the tissue material and physiological responses and functions.

Before a type of energy source or imaging modality is selected, it is important to understand the nature of physiological information needed for image formation. In other words, some basic questions about the information of interest should be answered. What information about the human body is needed? Is it anatomical, physiological, or functional? What range of spatial resolution is acceptable? The selection of a specific medical imaging modality often depends on the type of suspected disease or localization needed for proper radiological diagnosis. For example, some neurological disorders and diseases demand very high resolution brain images for accurate diagnosis and treatment. On the other hand, full-body SPECT imaging to study metastasizing cancer does not require sub millimeter imaging resolution. The information of interest here is cancer metastasis in the tissue, which can be best obtained from the blood flow in the tissue or its metabolism. Breast imaging can be performed using X- rays, magnetic resonance, nuclear medicine, or ultrasound. There is no perfect imaging modality for all radiological applications and needs. In addition, each medical imaging modality is limited by the corresponding physics of energy interactions with human body (or cells), instrumentation, and often physiological constraints. These factors severely affect the quality and resolution of images, sometimes making the interpretation and diagnosis difficult. The following Figure 2.2 gives a generic block diagram of a typical modern electronic medical imaging system.

2.2. Transmission and Emission Tomography

Transmission tomography and Emission tomography are the two main families of medical imaging. X-rays belongs to the first family, where the radiation source is outside the patient, while Nuclear medicine belongs to the second family, where the radiation source is inside the patient. Transmission tomography investigates a semi-transparent object by sending radiation through it from a number of angles. The projections are then fed to a computer and the amount of absorption is reconstructed. X-ray CT (computed tomography) uses transmission measurements to estimate a cross-sectional image within the patient body.

X-rays have very high energy, and they are able to penetrate the patient body. However, not every X-ray can make it through the patient body. Some X-rays get scattered within the body, and their energy gets weakened. During X-ray scattering, an X-ray photon interacts with an electron within the patient, transfers' part of its energy to that electron, and dislodges the electron. The X-ray is then bounced to a new direction with decreased energy. Some other X-rays completely disappear within the body, converting their energy to the tissues in the body, for ex., via the photoelectric conversion. The photoelectric effect is a process in which the X-ray photon energy is completely absorbed by an atom within the patient. The absorbed energy ejects an electron from the atom. Energy deposition within the body can damage DNA if the X-ray dose is too large.

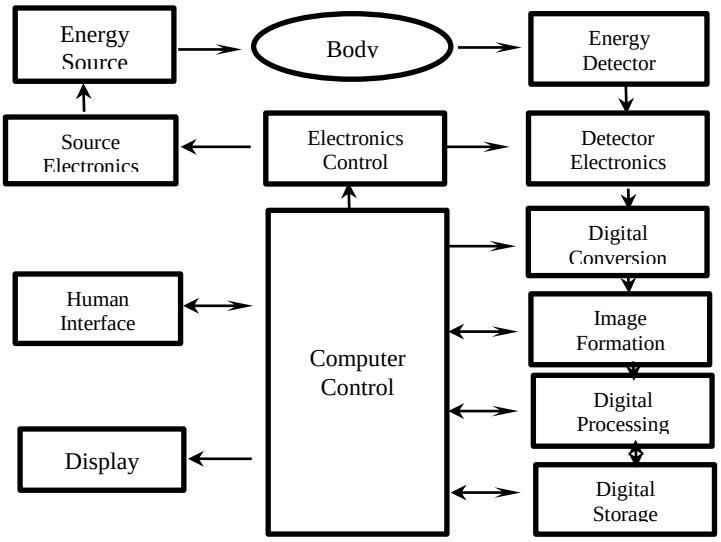

Fig. 2.2. Generic Block diagram of a typical modern electronic medical imaging system (S. Tiwari et. al., 2013).

Emission tomography is a medical imaging modality that can provide unique functional information about physiological processes in the body. Typically, a small amount of a radioactive compound (or radiotracer) is introduced into a subject via injection or inhalation. Sometimes the radiotracer itself is of physiological interest as in ^{15}O imaging in the brain. In other situations, the radioisotope is attached to a molecule that is selectively taken up in different anatomical regions, such as ^{18}F labeled fluorodeoxyglucose (FDG) in tumors. After allowing the radiotracer to distribute throughout the body, an image of the radiotracer distribution can be made. This image indicates the concentration of the radiotracer in different anatomical regions. This is important for diagnosis, for example, in cancer studies, since tumors tend to use more glucose than other regions in the body. Therefore, FDG images often show "hot spots" or regions of higher concentration where tumors lie. In other studies physicians are interested in "cold spots" due to improper blood circulation (Joseph, 2003).

In transmission tomography, X-ray tomography for instance, the source's position is known so that every collected photon yields exact information about the projection line that is the line joining the detection incidence and the source. This is not the case in emission tomography where the activity distribution, the emitting source of photons, is the unknown. To extract information about the spatial distribution of the activity, a collimator is used.

Another difference between X –ray imaging and nuclear medicine imaging is that we have a smaller amount of detected photons in the latter (P. Sustens, 2002). Thus noise is a big player in this process and must be taken care of; hence stochastic modelling becomes very useful. We cannot predict the exact amount at which the atom will disintegrate; however we know the decay probability as

$$\frac{dN(t)}{dt} = -\beta N(t)$$

Where β is an isotope dependent decay constant and N(t) is the activity at time t. This differential Eq. gives away the expected value as

$$N(t) = N(t_0)e^{-\beta(t-t_0)}$$

Since the process is statistical, we usually measure only an approximation to the true N(t). In the next Section 2.3, we present an overview of medical image reconstruction algorithms, brief discussion about various categories of reconstruction algorithms their principles, mathematical models benefits and limitations.

2.3. Medical Image reconstruction Overview

The main aim of image reconstruction in CT/PET is to represent the internal structure of a subject based on the detection of the radiation emitted by the subject's body after introducing a radiopharmaceutical. This process can take place in 2D or 3D acquisition modes and 2D or 3D reconstruction algorithms can also be employed. Different kind of reconstruction algorithms can be used (analytical or iterative) depending on several parameters such as the desired signal-to-noise ratio, the static or dynamic character of the tracer's distribution, the computational power and last but not least, the clinical task. In other words, one can say that there is not an optimal image reconstruction algorithm.

The problem of image reconstruction in CT/PET is shown schematically in Figure 2.3. A pair of gamma rays is emitted by the subject and it is registered by a detector tube. Each detector tube can detect gamma rays occurred inside the volume formed by the surfaces of detectors. This volume has the shape of an elongated parallelepiped and is referred as a *tube of response*.

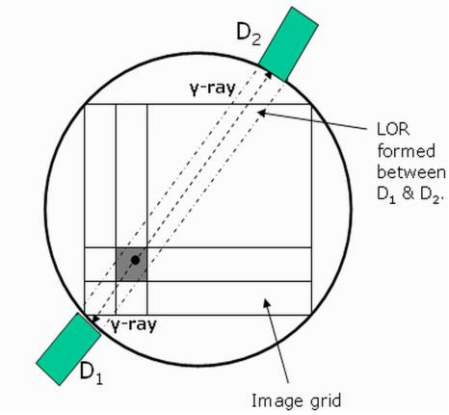

Fig. 2.3. The coincidence data detected in each LOR estimate the activity density in the image.

At the end of the PET scanning a number of gamma rays have been identified by each pair of detectors. This information represents the radioactivity in the subjects viewed by different angles. For the reconstruction of the activity density inside the subject using the data (projections) recorded in each detector tube, a reconstruction algorithm must be used. Next, a digital image is formed and the value of each pixel (or voxel) is proportional to the activity density of the area correspond to the pixel (or voxel).

In literature, various image reconstruction algorithms are developed in the last few decades. These are mainly divided into two classes, namely analytical methods (Per Christian Hansen et. al., 2012) and iterative techniques (Marcel Beister et al., 2012). Analytical methods based on a continuous sampling and the reconstruction process consists of the direct inversion of the measurement Eq. using the Radon transform (J. Radon, 1917). The most frequently used in this category is the filtered back-projection algorithm (FBP) (J. Devaney, 1982). This algorithm is fast but it provides poor image quality, streak artifacts and low signal-to-noise ratio because of limited number of projection sets. On the other hand, the iterative techniques can be modified to preserve the intricate details of the images and are far more immune to noise when compared to their counterparts iterative methods are based on iterative error correction techniques. There are different ways to implement these iterative methods. The main difference depends upon initial guess matrix, computation of the projections, physical correction models (scattering, random, attenuation, etc.), and the error corrective update computation in the estimated projections (Green PJ *et. al.*, 1990).These iterative reconstruction methods are classified into two categories namely, classical iterative algebraic reconstruction methods and statistical iterative reconstruction methods. The classical algebraic reconstruction techniques (ART), first proposed by (Gordon *et al.*, 1970), relied on Kaczmarz's iterative projection method (Kaczmarz S et al., 1937). However, the reconstruction using classical ART method deteriorated by a striping effect that made it sensitive to measurement noise. (Gilbert, 1972) proposed to quadratic optimized the ART methods to correct the sensitivity to noise using the simultaneous iterative reconstruction technique (SIRT), where the pixel updates due to all rays were accumulated, and their averages applied to each pixel only at the end of the iteration. This led to

good noise suppression, but resulted in slow convergence rates. (Andersen *et al.*, 1984) proposed that the all the acquired pixels updates for only one view at a time. This algorithm effectively combined the higher convergence rate of ART with the quadratic optimized SIRT methods, and is known as the simultaneous algebraic reconstruction technique (SART). Some other methods also have been used to solve ART methods such as component averaging methods (CAV) (Fernández J *et al*., 2002), block-iterative CAV (BICAV) (R. Vijayarajan, 2014), the multiplicative algebraic reconstruction technique (MART) (Marcel Beister *et al*., 2012).

SIR method have shown great potential to replace traditional analytical methods like FBP which take into account of statistical properties of the data have been shown to be superior in suppressing noise and streak artifacts. Statistical iterative reconstruction (SIR) (Qi J *et. al.*, 2006) methods reconstruct images by iteratively maximizing likelihood function. Examples are MLEM (Shepp and Vardi, 1982), Median Root Prior (MRP) (Alenius S, Ruotsalainen, 1989), Ordered Subsets Expectation Maximization (OSEM) (Hudson and Larkin, 1994) and their variants (Fessler, 2006).

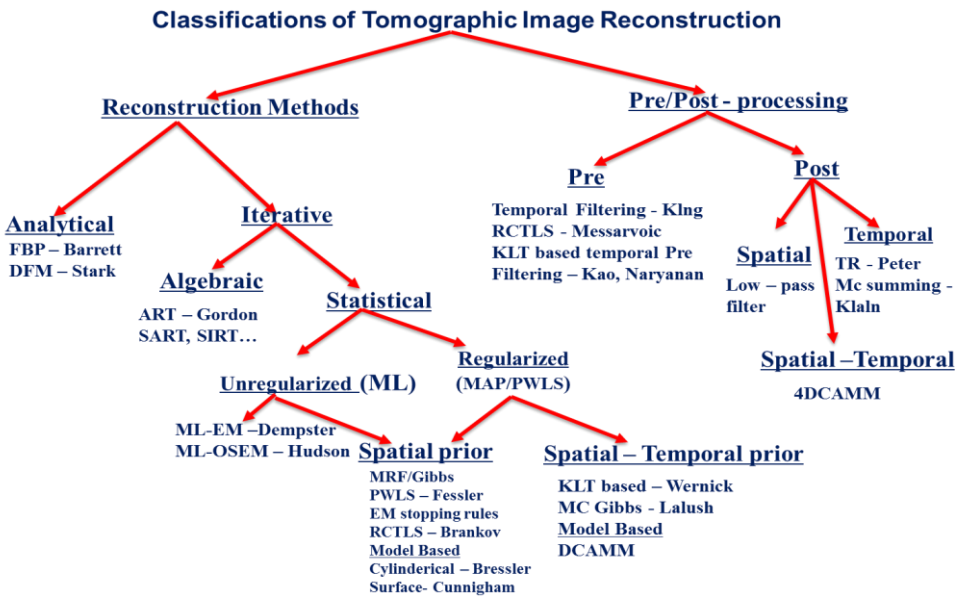

Fig. 2.4 Classifications of Tomographic Image Reconstruction Techniques

Abbreviations

ART – Algebraic Reconstruction Technique

CAMM – Content adaptive Mesh Modeling

MRF – Markov Random Field

ML – Maximum Likelihood

DCAMM – Deformable CAMM
DFM – Direct Fourier Method
EM – Expectation Maximization
FBP – Filtered Back Projection
KLT – Karhunen – Loeve Transform
MAP – Maximum a posterior
MC – Motion Compensation
OSEM – Ordered Subsets EM
PWLS – Penalized weighted least squares
RCTLS – Regularized total least square
TR – Temporal Regression

It plays an important role on the quality of the images produced by PET/SPECT since they can perform better with noisy, incomplete data, accurate system modeling, image prior knowledge, and as an alternative to both the analytical and algebraic methods, being less sensitive to noise and sparse view inputs. However, the major drawbacks associated with statistical algorithms are their slow convergence, the choice of an optimum initial point, and ill-posedness. The diagrammatically classification of Image reconstruction methods are shown below in Figure 2.4. The next Section, presents detail discussion about analytical methods (such as: Filtered back-projection (FBP) etc.) of medical image reconstruction algorithms.

2.3.1. Analytical methods

The role of image reconstruction is to use the data collected by the detectors to form the image of the object. There are two main approaches to the image reconstruction. The first is the *analytic* and uses the mathematics of computed tomography relating the coincidence data detected in each detected tube with the activity distribution in the object. Typical examples of these algorithms are the Fourier methods and the filtered back-projection algorithms. The second approach is the *iterative methods* that model the data collection process and attempt to find the best image that is most consistent with the measured data. The iterative algorithms will be analyzed in the next section.

A line integral represents the integral of some parameters of the object along a line. If the coordinate system of the Figure 2.5 is used, each line integral is represented by (θ, t) parameters and the object by the 2D function $f(x, y)$.

The Eq. of line AB is as follows:

$$x\cos\theta + y\sin\theta = t \tag{2.1}$$

and the line integral $P_\theta(t)$ is defined as follows:

$$P_\theta(t) = \int_{(\theta,t)line} f(x,y)\,ds \tag{2.2}$$

Figure 2.3 represents the geometrical configuration of the 2D image reconstruction. The 2D object is represented by *f(x, y).* It is mathematical preferable to formulate the problem in terms of the rotated coordinate system *(t, s).* In the *(t, s)* system the origin is the same with the origin of the *(x, y)* system.

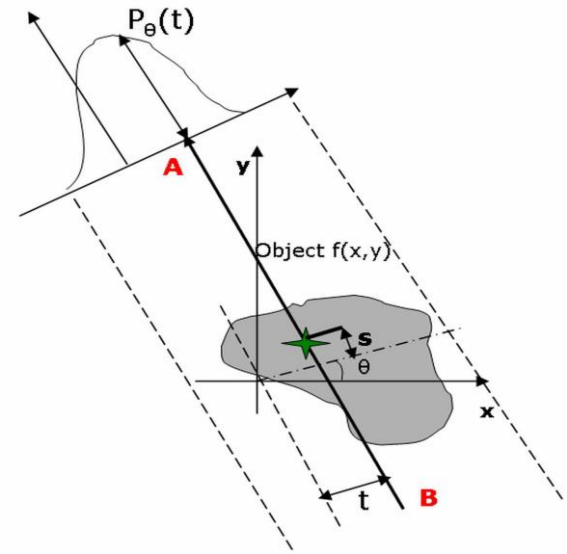

Fig. 2.3: The 1D projection at angle θ, is an integral of the object distribution *f(x, y)* along the *s* direction.

Using a delta function, the Eq. (2.2) can be rewritten as:

$$P_\theta(t) = \int_{-\infty}^{\infty}\int_{-\infty}^{\infty} f(x,y)\,\delta(x\cos\theta + y\sin\theta - t)\,dxdy \tag{2.3}$$

Eq. (2.3) defines the 2D *Radon transform* of *f(x,y).* It specifies the 1D projection of *f(x,y)* at the projection angle θ. The problem of image reconstruction is to try to find the solution of 2D *inverse Radon transform*.

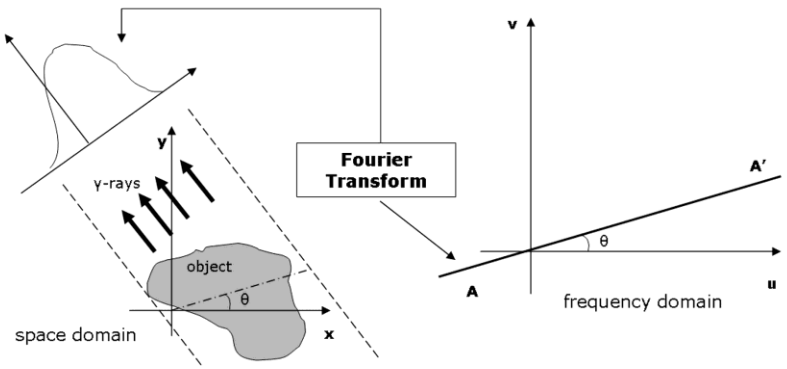

Fig. 2.6: The Fourier slice theorem.

In other words the aim is to find the 2D object distribution *f(x,y)* given the set of 1D projection data, $P_\theta(t)$ obtained at different projection views, θ. If the 2D Fourier transform of the object function is defined as follows:

$$P_\theta(v_t) = \int_{-\infty}^{\infty}\int_{-\infty}^{\infty} f(x,y)e^{j2\pi(ux+vy)}dxdy \qquad (2.4)$$

which is the Fourier Transform (FT) of *f(x,y)* along the t-axis. Eq. (2.4) is the *Fourier slice theorem* in image reconstruction from projections which is the basis of image reconstruction. The Fourier slice theorem mentions that the 1D Fourier transform of a projection at angle θ is equal to the 2D Fourier transform of the image evaluated along a radial profile at angle θ with respect to the x-axis. This is schematically shown at Figure 2.6.

Here, a brief summary of filtered backprojection (FBP) method is given below:

- Get the 1D Fourier transform of the first projection angle of the sinogram.
- Multiply it by the filter function.
- Get the inverse Fourier transform.
- Back-project the filtered projection.
- Repeat for all angles around the object.

The FBP algorithm has several advantages over Fourier transform methods (Kak and Slaney, 1987). In FBP the reconstruction procedure can be applied as soon as the first projection has been acquired. In this way the reconstruction is speed up and reduces the amount of data that must be stored. Secondly, it is more accurate to perform interpolation in the space domain than in frequency domain.

In the next section, discussion about iterative methods is presented. Iterative reconstruction algorithms produce accurate images without streak artifacts as in filtered backprojection. They allow improved incorporation of important corrections for image degrading effects, such as attenuation, scatter and depth-dependent resolution. Only some corrections, which are important for accurate reconstruction in CT, PET, and SPECT, can be applied to the data before filtered backprojection. Figure 2.7, shows the output of standard Shepp-Logan head phantom using without filter and with filter backprojection method with various degree of projection angles. The main limitation for introducing iterative algorithms in nuclear medicine has been computation time, which is much longer for iterative techniques than for filtered backprojection. Modern algorithms make use of acceleration techniques to speed up the reconstruction. These acceleration techniques and the development in computer processors have introduced iterative reconstruction in daily nuclear medicine routine.

2.3.2. Iterative methods

As an alternative to back-projection reconstruction a large family of reconstruction methods under the name *iterative methods* is often employed in image reconstruction especially in the area of emission tomography. The first method of this kind is the *algebraic reconstruction techniques* (ART) and it was first used in the EMI brain CT scanner developed by Sir G. Hounsfield (Hounsfield, 1973).

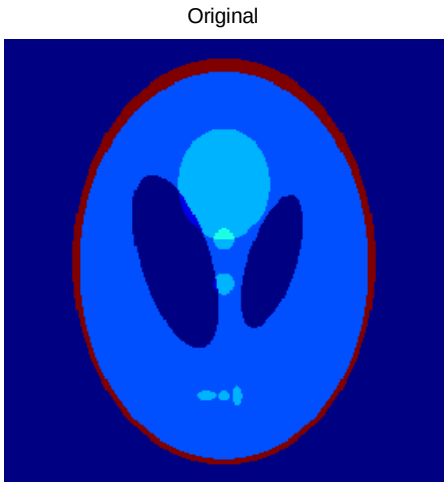

(a)

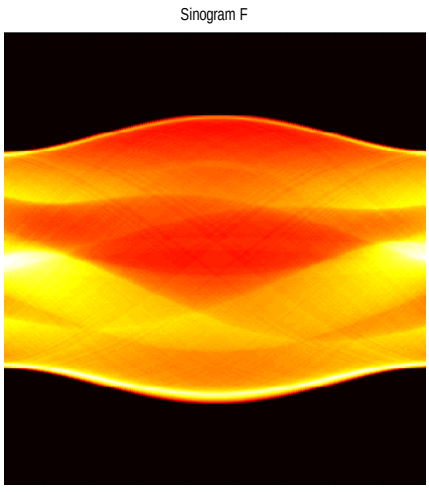

(b)

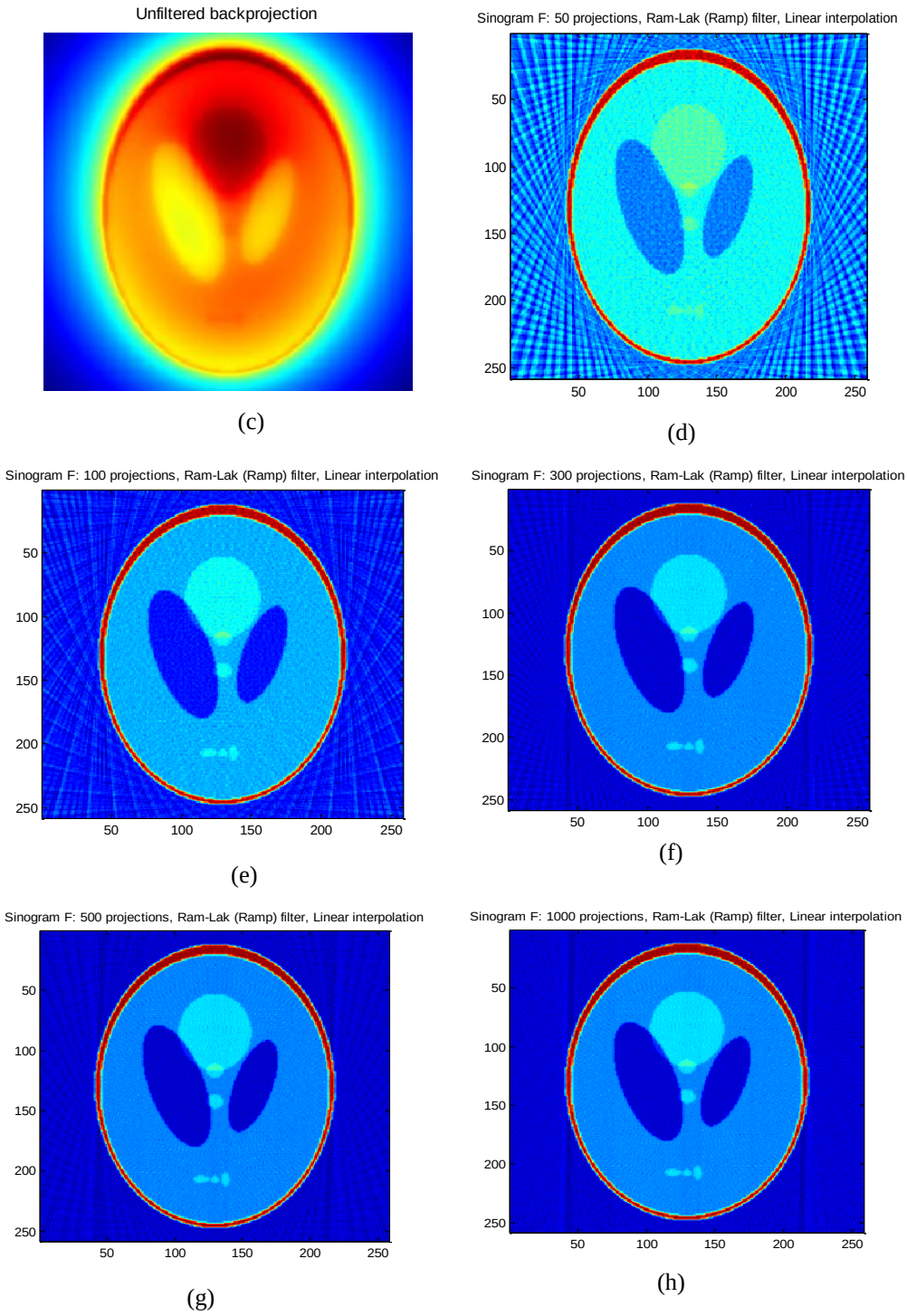

Fig. 2.7: (a) Original Shepp-Logan head Phantom, 256 × 256. (b) Sinogram over 1000 projections, i.e. the projections are (vertically) stacked together such that each row contains a projection from a different angle θ. (c) Reconstruction obtained without filter, (d)-(h) Reconstructions obtained with our implementation of the filtered backprojection algorithm. For each experiment, the number of projections has been increased. However, projection were always taken equally spaced over 180 degrees: (d) 50, (e) 100, (f) 300, (g) 500, and (h) 1000 projections.

In ART (Gordon *et. al.* 1970, Gordon 1974) it is assuming that the cross section consists of an array of unknowns and algebraic Eq.s for the unknowns have to be set up for these unknowns in terms of the measured projection data. This kind of image reconstruction totally differs from the previous described methods because the problem is discretized in the very early steps, whereas in the transform methods the discretization occurs at the last step of the computer implementation (Censor, 1983). The ART methods are aiming to solve the discrete reconstruction problem. This is the problem of estimating an image vector ***x*** where ***y*** is the projection vector:

$$y = Ax \tag{2.5}$$

where ***A*** is the projection matrix and it relates the image vector ***x*** with the projection vector ***y***. This iterative method produce a sequence vector $x^{(0)}$, $x^{(1)}$, $x^{(2)}$,… such that converges to $\hat{x}$. The progress of producing $x^{(k+1)}$ from $x^{(k)}$ is referred as an iterative step. In Figure 2.4 an object *f(x,y)* is shown and it is superimposed by an image grid. In PET case each value of *f(x,y)* represents the activity density inside the source. Let x_i denotes this value of the i^{th} pixel and let *N* be the total number of image pixels. *A* ray is a straight line that connects the surfaces of two opposite detectors (detector tube) and corresponds to the line integral over the region of the source covered by the ray. This line integral is called as a *ray-sum*.

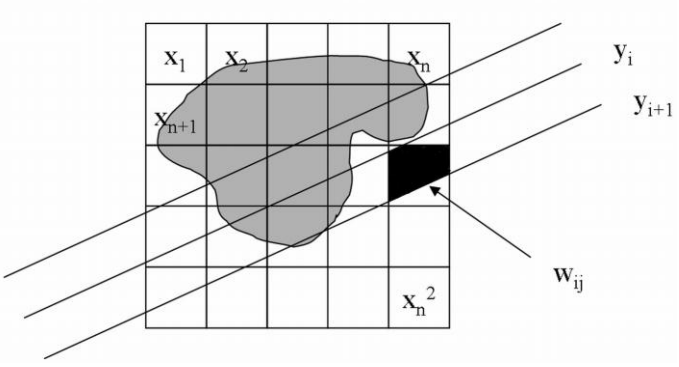

Fig. 2.8: Reconstruction process in algebraic method.

Each ray ***y*** overlaps a pixel with specific value. These overlapping areas are named weighting functions w_{ij}, representing the area covered between a pixel and two adjacent rays. The most of the w_{ij} factors are zero.

If y_j is the ray-sum measured along the j^{th} ray, the relationship between the image vector x and the ray-sum vector y can be expressed as:

$$y_j = \sum_{i=1}^{M} x_i w_{ij}, \quad j = 1, 2, ...N \tag{2.6}$$

where M is the total number of detector tubes and the coefficient w_{ij} is a weighting factor that expresses the contribution of the i^{th} pixel to the j^{th} line integral. This factor can be expressed by the shadow area, as it is shown in Figure 2 .8. The solution of the Eq. (2.5) is not very easy because N and M are large numbers and hence the required computer memory is extremely large. Furthermore, conventional matrix inversion methods cannot be used considering the dimensions NxM of the w_{ij} matrix. To solve this problem iterative algorithms have been developed. According to those algorithms, the Eq. (2.6) can be thought as M linear Eq.s with N unknowns. Each one of those Eq.s represents a hyper plane in the N-dimensional space of images. When a unique solution is feasible, the intersection of all these hyper planes is a simple point giving that solution. Additionally, the projection data y_j are corrupted by noise and no unique solution exists for the problem, but the solution rather will oscillate in the neighborhood of the intersections of the hyper planes. The iterative scheme works by checking the consistency of the Eq.s for iteratively different x_i values. The choice of the initial guess of x_i values is very critical in the behaviour of these algorithms. The convergence rate to the solution also depends on the angles between the hyper planes. If the M hyper planes could be made orthogonal with respect to each other, the correct solution would be arrived at with only one pass through the M Eq.s. In this case it is assumed that no noise exists. Iterative algorithms have the drawback that high computational effort is needed but they have some advantages such as:

- General applicability to a wide range of problems.
- Applicability to standard numerical analysis technique.
- Applicability to 2D or 3D.

Although this type of algorithm widely used in the past, nowadays iteration methods based on statistical properties such as maximum likelihood

are more useful. In other words, iterative algorithms can be classified into two categories. The first category contains the conventional iterative algebraic methods which reconstruct the images using Eq. (2.6) algorithms that will be further explained in the next section.

2.3.2.1. Algebraic methods

The next categories belong to algebraic reconstruction techniques, like Algebraic Reconstruction Technique (ART) [Gordan et. al. 1970], Simultaneous Iterative Reconstruction Technique (SIRT) (Gilbert, 1972) and Simultaneous Algebraic Reconstruction Technique (SART) (Anderson & KaK, 1984). Unlike transform methods, algebraic methods do not require complete set of uniformly distributed projections for precise reconstruction and they are also more stable under noisy conditions (Marabini et. al. 1998). Furthermore, they allow using a priori information in reconstruction process (Green PJ *et. al.,* 1990). However, algebraic techniques are computationally very demanding and until recently, they were not able to compete with transform methods. In this section, we explain the basic concepts behind algebraic methods and explain the difference between ART, SIRT, and SART.

- **Principle of Algebraic Techniques**

We first provide common algorithm for ART, SIRT and SART and then we briefly describe each of this method separately to enhance the differences between them as well as their pros and cons. The pseudo code for general algorithm is shown in Table 2.1. We denote the initial estimate of the volume as $x_{(0)}$ and until we reach given termination criterion we iterate over all pixels p_i from all projections P. The pixels are divided into m subsets S and for each subset we compute new estimate of the volume. The update of the volume can be split into three phases: forward projection, compare step and back projection. In forward projection we simulate the acquisition of real projection. For each pixel we generate one ray and trace its path through the volume gathering value and weight of each voxel hit by the ray. In that way we obtain so called virtual projection for each pixel (see Figure 2.4). In the correction step we compute for each pixel the error of its virtual projection towards its real value. Finally, in back projection we

correct value of each voxel according to calculated errors of all pixels that contribute to given voxel. After processing all pixels from given subset we obtain new estimate of the volume. In other words, the volume estimate x^k, where *k* denotes number of updates, is obtained as a function of x^{k-1} and subset *S*. Keep in mind, that in general one update does not form one iteration of the algorithm. The way in which they are divided into subsets forms the difference between ART, SIRT and SART.

Table 2.1: General algorithm for algebraic techniques

```
Initialize volume
Split pixels into subsets
Until converges repeat
    For all subsets do
        For all pixels from subset do
            Forward projection
                %compute virtual projection
            Compare step
                %compute error
            Back projection
                %update volume according to the error
```

- **ART**

In ART one subset S contains only one pixel. The volume is thus updated after one pixel is processed. For a voxel x_j we can describe the update step by the Eq.:

$$x_j^k = x_j^{k-1} + \lambda \left(\frac{P_i - \sum_{n=1}^{N} w_{in} x_n^k}{\sum_{n=1}^{N} w_{ij}^2} w_{ij} \right) \qquad (2.13)$$

where initial estimate x^k, weighting functions w_{ij}, representing the area covered between a pixel and two adjacent rays, *M* is the total number of rays and *N* is the total number of pixels of all projections *P*, λ is a relaxation factor from (0, 1].

The ART is relatively fast but the quality of the results is not that high. Reconstructions usually suffer from salt and pepper noise and also contain some artifacts (Anderson and Kak, 1984).

- **SIRT**

To improve the quality of the reconstructions simultaneous iterative reconstruction technique (SIRT) was presented by Gilbert in (Gilbert, 1972). In the SIRT one subset S contains allpixels from all projections. Thus, the volume update corresponds to one iteration of the algorithm and for one voxel can be expressed as:

$$x_j^k = x_j^{k-1} + \frac{\lambda}{\sum_{P_i \in P} w_{ij}} \sum_{P_i \in P} \left(\frac{P_i - \sum_{n=1}^{N} w_{in} x_n^k}{\sum_{n=1}^{N} w_{in}} w_{ij} \right) \quad (2.14)$$

Compared to ART, the results of SIRT are better but the convergence is significantly slower.

- **SART**

Andersen and Kak presented simultaneous ART (SART) in (Anderson and Kak, 1984) as a compromise between ART and SIRT. In SART, one subset *S* contains all pixels from one projection view P_φ at an angle φ. For a voxel x_j this update can be expressed as:

$$x_j^k = x_j^{k-1} + \frac{\lambda}{\sum_{P_i \in P_\varphi} w_{ij}} \sum_{P_i \in P_\varphi} \left(\frac{P_i - \sum_{n=1}^{N} w_{in} x_n^k}{\sum_{n=1}^{N} w_{in}} w_{ij} \right) \quad (2.15)$$

where λ is known as the relaxation parameter, and *N* is the total number of pixels. The process of iteration first guesses the values of the pixels and then alters these values until it is correct one. All the Eq.s belonging to the same angle at the same time ($P_i \in P_\varphi$) are used before comparing the new values of the pixels with the old one. Furthermore, it has been pointed out that SART can be improved by adjusting the relaxation parameters [9]. Careful selections for the relaxation parameters can lead to the better qualities of reconstructions [41- 44]. Here, we choose the value of λ as less than one, and find good convergence with small number of iterations. In each iteration of SART, all the pixels with the same weights receive the same corrections even they have different gray levels. The rate of convergence of a SART based reconstruction approach is faster, but the quality of reconstructed image is not better with respect to statistical (e.g. MLEM) approach.

2.3.2.2. Statistical methods

The next category contains the iterative statistical reconstruction methods which reconstruct an image by maximizing the likelihood function. The most known example of the statistical methods are the Maximum Likelihood Expectation Maximization (MLEM) (Shepp and Vardi 1982, Dempster et. al. 1977) and its modified version of Ordered Subsets Expectation Maximization (OSEM) (Hudson and Larkin, 1994) algorithms that will be further explained in the next section.

- **Expectation Maximization algorithms for PET**

The basic aspects of image reconstruction were presented in the previous chapter. Analytical methods have been historically the most commonly used reconstruction methods in PET. Consequently a method for image reconstruction that would incorporate the stochastic nature of the emission process could produce better images than conventional analytical techniques. Iterative image reconstruction algorithms offer this approach. The algorithms that are examined and presented in this thesis are based on statistical maximum likelihood estimation techniques. *Likelihood* is a general statistical measure that is maximized when the difference between the measured and estimated projection is minimized. **Expectation–Maximization** (EM) algorithm presented by (Dempster *et. al.* 1977) is a general iterative method.The basic working details of EM algorithms are as follows:

Shepp and Vardi published an implementation of the EM algorithm adapted to the problem of image reconstruction in PET (Shepp et. al. 1982). This is called as *Maximum Likelihood Expectation Maximization* (MLEM). The name of the MLEM algorithm derives from the fact that there is an *expectation step* that uses current parameter estimates in order to apply a reconstruction of the unobservable Poisson process. The first step is followed by a *maximum likelihood* that uses this reconstruction to revise the parameter estimates. The maximum likelihood approach in image reconstruction for emission tomography was first introduced by Rockmore and Macovski (Rockmore et. al. 1976). Shepp and Vardi created a mathematical model including the physics of positron emission. The MLEM algorithm

estimates an unknown density distribution in the source from the measured counts. Using the proposed mathematical model, it is possible to calculate the probability that any initial distribution density of the object under examination could have produced the measured data. In the set of all produced images, the image having the highest probability is the maximum likelihood estimates of the original project. The MLEM requires multiple iterations depending on the scanner geometry and the measured data to reach to an acceptable image.

In positron emission tomography a radioactive isotope is introduced in the body and forms an unknown emitter density. Emission then occurs according to Poisson statistics. When two photons are emitted, they are detected in coincidence by a pair of detector elements which forms a detector tube. The set of counts collected is represented by the vector *[y(1), y(2), y(3),…., y(J)]* where *y(j)* is the total number of coincidences counted in the j^{th} detector tube and *J* is the total number of detector tubes. If *N* is the total number of detector elements then the total number of detector tubes is *J = N(N - 1)/2*. The problem here is to estimate the emission density from the data vector y(j). For purpose of display and computer implementation, the density *f* is discretized into pixels *i=1, 2,…, I.* This discretization has been followed in this thesis as well. In each pixel *i* there is an unknown count $\hat{x}(i)$, with mean $x(i) = E\left[\hat{x}(i)\right]$, *i = 1, 2,…, I.* In other words the problem *is to estimate x(i) from the observed data y(j), j=1, 2, 3,, J.*

The mathematical model described by Shepp and Verdi was based on the hypothesis that the emission in the source (pixel) occurs according to Poisson statistics. In each pixel *i* there is a Poisson distributed number *x(i)* with mean *x(i)* that can be generated independently (Shepp et. al.1982):

$$P\left(\hat{x}(i) = m\right) = e^{-x(i)} \frac{x(i)^m}{m!}, \text{ m=0, 1, ….} \qquad (2.16)$$

Here, it is assumed that each emission in pixel i is detected by detector tube j with known probability:

$$a(i,j) = P(\text{event detected in tube } j \mid \text{event emitted in pixel } i) \qquad (2.17)$$

where the *a(i,j)≥0*. The transition matrix *a(i,j)* is assumed to be exactly known. It strongly depends on the PET scanner's and detector array geometries. Therefore, the probability of an event emitted in pixel *i* to be detected by any detector tube, it is given by:

$$a(i) = \sum_{j=1}^{J} a(i,j) \leq 1 \qquad (2.18)$$

The inequality of Eq. (2.18) expresses the fact that parts of the gamma-rays emitted go undetected by the PET scanner. (Shepp and Vardi, 1982) commented that with no loss of generality, it can be assumed that all photons are detected and hence the equality holds on the Eq. (2.18). Hence the transition matrix *a*, is the (conditional) probability that a *detected* photon emitted in pixel *i* is detected in detector tube *j* and satisfies:

$$a(i) = \sum_{j=1}^{J} a(i,j) = 1 \qquad (2.18a)$$

This is equivalent to thinking that *f(x, y)* is the activity density of the emitted counts *which are detected.*

To continue the mathematical discussion, it is noted that the variables y(j) are independent and Poisson with expectation $\tilde{y}(j)$ where:

$$\tilde{y}(j) = E\left[y(j)\right] = \sum_{i=1}^{I} x(i)a(i,j) \qquad (2.19)$$

Since *x(i)* are independent Poisson variables, a linear combination of these variables, as the one in the Eq. (2.17), is also Poisson distributed. Based on this, the likelihood function is given by:

$$L(x) = P(y|x) = \prod_{j=1}^{J} e^{-\tilde{y}(j)} \frac{\tilde{y}(j)^{y(j)}}{y(j)!} \qquad (2.20)$$

The likelihood function *L(x)* represents the *probability under the Poisson probability model for emission to observe the given counts in detector tubes if the true density is x(i).* If the log-likelihood of Eq. (2.20) is tak-

ing into consideration and using also the Eq. (2.19), the maximum likelihood is:

$$l(x) = \log\left(L(x)\right) = \sum_{j=1}^{J}\sum_{i=1}^{I} x(i)a(i,j) + \sum_{j=1}^{J} y(j)\log\left(\sum_{i=1}^{I} x(i)a(i,j) - \sum_{j=1}^{J}\log y(j)!\right) \tag{2.21}$$

Taking the first and second derivatives of the log-likelihood function, it can be shown (Vardi et. al. 1985) that the matrix of second derivatives is negative semidifinite and *l(x)* is a concave function. Consequently, sufficient conditions for a vector $\hat{x}$ to be a maximizer of *l* are the following condition:

$$0 = x(i)\frac{\partial I(x)}{\partial x(i)_{\hat{x}}} = \hat{x}(i) + \sum_{j=1}^{J}\frac{y(j)\hat{x}(i)a(i,j)}{\sum_{i'=1}^{I}\hat{x}(i')a(i',j)} \tag{2.22}$$

where *i=1,2,...,I* and *j=1,2,...J*. The formula of EM can now be derived by solving the Eq. (2.22).

The EM algorithm is given as follows:

(a) *Start with an initial guess* x^0 *satisfying* $x^{(0)}(i)>0$, *i=1,2,....,I*

(b) *If* $x^{(k)}$ *denotes the estimate of x after k iterations, define a new estimate* $x^{(k+1)}$ *where:*

(c) $$x^{(k+1)}(i) = x^{(k)}(i) + \sum_{j=1}^{J}\frac{y(j)a(i,j)}{\sum_{i'=1}^{I} x^{(k)}(i')a(i',j)} \quad i=1,2,....,I \tag{2.23}$$

(d) *If the required accuracy for numerical convergence has been achieved then stop the iteration process.*

The Eq. (2.23) is the expression of the EM algorithm that can be directly applied to the PET image reconstruction problem. Furthermore:

$$\tilde{y}^{(k)}(j) = \sum_{i'=1}^{I} x^{(k)}(i')a(i',j) \tag{2.24}$$

where $\tilde{\tilde{y}}^{(k)}(j)$ is the reprojection of the estimated image vector $x^{(k)}$ at the k^{th} *i*teration to the data space vector. In other words $\tilde{y}^{(k)}$ contains the expected values of the measured data if the estimated image vector $x^{(k)}$ were the actual activity density $\hat{x}$ in the source. Hence, the general form of the update process at the *(k+1)th* iteration is:

$$x^{k+1}(i) = x^{k}(i)C^{k}(i) \quad i=1,2,\ldots,I$$

(2.25)

where:

$$C^{(k)}(i) = \sum_{j=1}^{J} \frac{y(j)a(i,j)}{\sum_{i'=1}^{I} x^{(k)}(i')a(i',j)} \qquad (2.26)$$

- **Ordered Subset Expectation Maximization (OSEM) algorithm**

In the OSEM algorithm the projection data are grouped into *Ordered Subsets* (OS). The number of these subsets defines the OS level. Shepp and Vardi's EM algorithm (i.e. projection followed by back- projection) is then applied to each one of these subsets in turn. The resulting reconstruction from one subset is the starting image for use with the next subset. Consequently, an iteration of the OSEM algorithm is defined as a single pass through all the specified subsets. More iteration can be performed by passing through the same ordered subsets, using as initial point the reconstructed image produced in the previous iteration. Generally, one can say that the image obtained after *m* iterations over *n* subsets in the OSEM algorithm, has been observed to be visually similar with the image resulted after $m \times n$ iterations of MLEM algorithm over the complete data set. In the case of a PET/SPECT scanner, the set of counts collected is represented by vector *[y(1), y(2), y(3),…., y(j)]* where *y(j)* is the total number of coincidences that are counted in the j^{th} detector tube and *j* is the total number of detector tubes, such as in the case of MLEM algorithm. The image is defined to be the vector *x [x(1), x(2), x(3),….,x(i)., x(N)]* , where *x(i)* is the total counts emitted by the i^{th} pixel and *N* is the total number of pixels.

Let x^0 be a uniform initial image, and $x^{(m)}$ be an estimation of the true activity distribution x after mth iterations. In addition, let S1, S2,…, Sn represent the nth subset to which the data vector y has been divided to. With the above definitions the mathematical formulation of the OSEM reads (Hudson and Larkin, 1994):

1. Start with an initial guess m=0, and $\hat{x}^m$, where $\hat{x}^m$ is system matrix with positive values, we need not put any non-negative constraints on the algorithm.

2. Repeat until convergence of $\hat{x}^m$

(a) $x^1 = \hat{x}^m$, $m = m+1$

(b) For subsets t = 1, 2,….., n

i. Projection Phase: Calculate expected values for cumulated counts y as:

$$\mu(j)^t = \sum_{i=1}^{I} a(i,j) \times (i)^t \text{ , for detectors } j \in S_n \qquad (2.27)$$

ii. Back-projection Phase: Calculate true activity distribution data as follows:

$$x(i)^{n+1} = x(i)^n \frac{\sum_{j \in S_n} \frac{y(j)a(i,j)}{\mu(j)^t}}{\sum_{j \in S_n} a(i,j)} \text{, for pixels i = 1,2,…, I.} \qquad (2.28)$$

(c) $\hat{x}^m = x^{n+1}$

In steps (a) to (c), y(j) represents the projected data in j^{th} line of response and *a(i, j)* is the system matrix element.

The general form of the update process at the m^{th} iteration is given by:

$$x^m(i) = x^{m-1}(i) C^{m-1}(i), \quad i = 1, 2, ...I \qquad (2.29)$$

Where: $$C(i)^{(m-1)} = \frac{1}{\sum_{j \in S_n} a(i,j)} \sum_{j \in S_n} \frac{y(j)a(i,j)}{\sum_{i'=1}^{I} x(i')^{(m-1)} a(i',j)} \qquad (2.30)$$

is a multiplicative coefficient that updates the image vector at the m^{th} iteration. The Eq. (2.28) shows that $C(i)^{(m-1)}$ depends only on the observed counts *y(j)* in each subset and on the system matrix element *a(i, j)* that corresponds to that pixel and line of response, the value of which is calculated once throughout this work, at initialization time. As clear from the above Eq., under the constraint that initial image $\hat{x}^0$ and system matrix are positive, we need not put any non-negativity constraint on the algorithm. According to Hudson and Larkin's paper, (1994) there are several options and some examples of them are:

1. *Non-overlapping subsets:* With *n* subsets each of *j* detectors per projection set $S1=\{1,2,\ldots,j\}$, $S_2=\{j+1,\ldots,2j\},\ldots,S_n=\{(n-1)j+1,\ldots,nj\}$ and continue to cycle in turn through each of these subsets. Data used in each sub-iteration comprises counts of all detected photons recorded on the first, second,…, last projection specified.
2. *Cumulative subsets:* Alternatively, set $S1=\{1,2,\ldots,j\}$, $S2=\{1,2,\ldots,2j\},\ldots,$ $S_n=\{1,2,\ldots,nj\}$. Cycle in turn through each of these subsets.
3. *Standard EM:* If all detectors grouped in one subset $S_1=\{1,2,\ldots,nj\}$, then the standard MLEM algorithm is provided.

Regarding the selection of subsets and order, Hudson and Larkin mentioned that since in PET all counts are collected simultaneously, OSEM can be applied after full collection of the counts. Then, tubes are rebinned in parallel groups defining projections. The order with which projections are processed is arbitrarily. Furthermore, if one wants to study a different algorithm than the OSEM, the backprojection step described in Eq. (2.26) would be replaced by this algorithm. Secondly, in Eq. (2.26) the image matches the activity expected to be recorded on the projection and the total count recorded on the projection:

$$\sum_{j\in S_n} y(j) = \sum_i \left(\sum_{j\in S_n} a(i,j) \right) x(i)^t \qquad (2.31)$$

However, initial scaling has no effect on the results of any subsequent iteration of EM algorithm. Finally, if the denominator in Eq. (2.31) is zero then $x(i)^{t+1} = x(i)^t$ is set.

- **Summary of Iterative methods**

Iterative image reconstruction methods have attracted considerable attention in the past decades for applications in positron emission tomography (PET) due to the feasibility of incorporating the physical and statistical properties of the imaging process more completely (Per Christian Hansen et. al., 2012; R. Vijayarajan et al., 2014). So far, all statistical reconstruction algorithms are based on the maximum likelihood (ML) or the least squares cost function. The maximum likelihood expectation maximization (MLEM) algorithm (Shepp and Vardi, 1982), which is a general statistical method for seeking the estimate of the image, allows computing projections that are close to the measured projection data. Iterative based ML reconstruction algorithms nevertheless require a considerable computational cost per iteration. An accelerated version of the MLEM algorithm, the ordered subsets EM (OSEM) was proposed by (Hudson *et al.*, 1984) to significantly improve the convergence speed in the PET reconstruction. This ordered subset principle has been then exploited in many algorithms for the same objective. Generally speaking, the tomography reconstruction with a limited number of data appears as a highly underdetermined ill-posed problem. The projection data generated by the PET system are initially noisy and the ML algorithm tends to increase this noise and in particular the noise artifacts through the successive iterations. This accumulation of noise leads to a premature stopping of the ML-EM reconstruction process. Several methods have been developed to decrease this accumulation of noise and improve the quality of the reconstructed images in tomography (Z. G. Gui *et. al.*, 2012; D. Kazantsev *et. al.*, 2012; Qian He *et. al.*, 2014; Hsiao I-T *et. al.*, 2003).

2.4. Literature survey

This section presents a brief review of related work in statistical image reconstruction techniques used in various medical imaging modalities with their brief description advantages and limitations as shown in Table 2.2.

Table 2.2: Brief overview of SIR methods
(Statistical Iterative Methods for Image reconstruction)

S.No.	Papers	BRIEF DESCRIPTION	ADVANTAGES	LIMITATIONS
1.	Maximum Likelihood Reconstruction for Emission Tomography. (Shepp and Vardi, 1982)	Previous models for emission tomography (ET) do not distinguish the physics of ET from that of transmission tomography. We give a more accurate general mathematical model for ET where an unknown emission density generates, and is to be reconstructed from, the number of counts n*(d) in each of D detector units d.	Within the model, we give an algorithm for determining an estimate lambda which maximizes the probability of observing the actual detector count data n over all possible densities.	Mathematically proof the Model. It also, not specifies a prior that leads to a more computationally feasible solution for PET.
2.	A theoretical study of some maximum likelihood algorithms for emission and transmission tomography (Lange, 1987)	This paper has the dual purpose of introducing some new algorithms for emission and transmission tomography and proving mathematically that these algorithms and related antecedent algorithms converge.	The Bayesian versions of the EM algorithms are shown to have superior convergence properties in a vicinity of the maximum.	Complex Mathematical model and theoretical convergence analysis. It also, not specifies a prior that leads to a computationally feasible modification.
3.	A Maximum A Posteriori Probability Expectation Maximization Algorithm for Image Reconstruction in Emission Tomography	The expectation maximization method for maximum likelihood image reconstruction in emission tomography, based on the Poisson distribution of the statistically independent components of the image and measurement vec-	The method is demonstrated to be superior to pure likelihood maximization, in that the penalty function prevents the occurrence of irregular high amplitude patterns in	The choice of the appropriate optimization criterion and reconstruction algorithm for emission tomography is

	(Levitan & Herman, 1988)	tors, is extended to a *maximum a posteriori* image reconstruction using a multivariate Gaussian a priori probability distribution of the image vector.	the image with a large number of iterations (the so-called "checkerboard effect" or "noise artifact").	worthy of further investigation.
4.	A generalized EM algorithm for 3-D Bayesian reconstruction from Poisson data using Gibbs priors (Hebert & Leahy, 1989)	A generalized expectation-maximization (GEM) algorithm is developed for Bayesian reconstruction based upon locally correlated Markov random field priors in the form of Gibbs functions and upon the Poisson data model.	The algorithm reduces to the EM maximum likelihood algorithm as the Markov random field prior tends towards a uniform distribution. Three different Gibbs function priors are examined.	This work shows that some improvement can be achieved for a wide range of regularization controller values, but statistical methods for optimizing the choice of this parameter are still needed.
5.	Bayesian reconstructions from emission tomography data using a modified EM algorithm. (Green, 1990)	A new method of reconstruction from SPECT data is proposed, which builds on the EM approach to maximum likelihood reconstruction from emission tomography data, but aims instead at maximum posterior probability estimation, that takes account of prior belief about “smoothness” in the isotope concentration.	A novel modification to the EM algorithm yields a practical method. The method is illustrated by an application to data from brain scans.	Manually set the controlling parameter beta value. Further work is needed to fine-tune the approach to various practical circumstances

6.	Scale-space and edge detection using anisotropic diffusion (Perona and Malik, 1990)	The scale space techniques introduced by within involves generating coarser resolution images by convolving the original image with a gaussian kernel. This approach has a major drawback: it is difficult to obtain accurately the locations of the 'semantically meaningful' edge at coarse scales. In this paper a new definition of scale space, and introduce a class of algorithms that realize it using a different process.	Results shows that it obtain a high quality edge detector which successfully exploit global information.	All parametric values set to manually like diffusion coefficient conductance (kappa) etc.
7.	Accelerated image reconstruction using ordered subsets of projection data, (Hudson & Larkin, 1994)	In this paper ordered subset expectation maximization algorithms for image reconstruction from projections is introduced. Ordered subset methods group the projection data into an ordered sequence of subsets (blocks). An integration of ordered subsets EM is defined as a single pass through all the subsets, in each subset using the current estimate to initialize application of EM with data subsets.	In simulation studies the OSEM provides an order of magnitude acceleration over EM, with restoration quality maintained.	This OS methods limited for only EM algorithm, it does not applied for other restoration algorithms.
8.	Bayesian image reconstruction for emission tomography based on	The aim of the present study was to investigate a new type of Bayesian one-step late reconstruction method which	The MRP method provided good-quality images with a similar resolution to the FBP	The optimum spatial resolution was achieved with

	median root prior. (Alenius & Ruotsalainen, 1997)	utilizes a median root prior (MRP). The method favors images which have locally monotonous radioactivity concentrations. The new reconstruction algorithm was applied to ideal simulated data, phantom data and some patient examinations with PET.	method with ramp filter and MLEM methods. The new MRP reconstruction method was shown to produce high-quality quantitative emission images with only one parameter setting in addition to the number of iterations.	rather small beta values, but not smaller than approximately 0.2 because of increasing spatial noise.
9.	A new convex edge-preserving median prior with applications to tomography (Hsiao *et. al.*, 2003)	The proposed method developed an entirely new class of convex priors that depends on data-fidelity term *f* and also on penalty term *m*, an auxiliary field in register with f. We specialize this class to our median prior (MP). The approximate action of the median prior is to draw, at each iteration, an object voxel toward its own local median. This action is similar to that of MRP and results in solutions that impose the same sorts of object properties as does MRP	The proposed method is an alternating algorithm to compute the joint MAP solution and apply this to emission tomography, showing that the reconstructions are qualitatively similar to those obtained using MRP.	In many simulations, they have not observed any dependence of the MAP solution on the initial estimate. Further work is required here. Also smoothness and positivity constrained solution to a tomographic MAP reconstruction will be further explore to derive novel and useful priors.
10.	Accurate image	In this work, we develop and	Numerical demonstra-	Further investi-

	reconstruction from few-views and limited-angle data in divergent-beam CT (Sidky *et. al.*, 2006)	investigate an iterative image reconstruction algorithm based on the minimization of the image total variation (TV) that applies to divergent-beam CT.	tions of our TV algorithm are performed with various insufficient data problems in fan-beam CT. The TV algorithm can be generalized to cone-beam CT as well as other tomographic imaging modalities.	gate and develop refinements were needed to the TV algorithm that optimize its performance.
11.	Prior image constrained compressed sensing (PICCS): a method to accurately reconstruct dynamic CT images from highly under sampled projection data sets (Chen *et. al.* 2008a)	In this paper, the spatial-temporal correlations in dynamic CT imaging have been exploited to sparsity dynamic CT image sequences and the newly proposed compressed sensing (CS) reconstruction method is applied to reconstruct the target image sequences. A prior image reconstructed from the union of interleaved dynamical data sets is utilized to constrain the CS image reconstruction for the individual time frames. This method is referred to as prior image constrained compressed sensing (PICCS).	The results indicate that PICCS enables accurate reconstruction of dynamic CT images using about 20 view angles, which corresponds to an under-sampling factor of 32.	Further studies are ongoing to investigate the final radiation dose reduction factor.
12.	Regularized image reconstruction with an anatomically adaptive prior for pos-	In this study, we explored an alternative approach to incorporating an anatomical prior into PET image reconstruction. In the proposed method,	This AAMDF smoothing prior was determined and applied adaptively to each anatomical re-	Proposed priors does not consider the anatomical functions of CT da-

	itron emission tomography (Chung Chan *et.al.* 2009)	regional information obtained from the anatomical prior was used to estimate an anatomically adaptive anisotropic median-diffusion filtering (AAMDF) prior.	gion on the emission image and then assembled to form a prior image for the next iteration in the reconstruction process.	ta. It's often restricted the limitations of the CT data, and the clinical value of this and other approaches involving anatomical priors in future studies.
13.	Regularization Parameter Selection Methods for Ill-Posed Poisson Maximum Likelihood Estimation (Johnathan M. Bardsley and John Goldes, 2010)	Regularized Poisson likelihood estimation has been studied extensively by the authors, though a problem of high importance remains: the choice of the regularization parameter.	Author present three statistically motivated methods for choosing the regularization parameter, and numerical examples will be presented to illustrate their effectiveness.	Theoretical analyses of DP, GCV, and UPRE are not discussed also non-quadratic regularization function such as Total variation extension is needed in this paper.
14.	An anatomically driven anisotropic diffusion filtering method for 3D SPECT reconstruction (Daniil *et. al.*	In this work, we propose an anatomically driven anisotropic diffusion filter (ADADF) as a penalized maximum likelihood expectation maximization optimization framework. The ADADF method has improved edge - preserving denoising charac-	The proposed method has an important ability to retain information which is absent in the anatomy. To make our approach more stable to the noise-edge classification problem, robust	It works well to preserve the edges and other fine structure details, dominant directions and frequency in the PET and SPECT. But, it

	2012)	teristics compared to other smoothing penalty terms based on quadratic and non-quadratic functions.	statistics have been employed.	cannot capable to preserve the collateral features (artifacts) created by true incidents (lesions).
15.	PML Algorithm for Positron Emission Tomography Combined With Nonlocal Fuzzy Anisotropic Diffusion Filtering (Zhiguo Gui et.al. 2012)	This work aims to improve the quality of PET images using a novel nonlocal fuzzy diffusion model. Compared to the PDE Median method, the proposed approach can impose an effective edge-preserving and noise-removing diffusion model for PET image reconstruction.	Experimental results showed that the proposed method is more effective in improving quality of reconstructed images comparing with other common methods like PL-ML, MRP.	Further works is needed to improve the visual quality for real clinical images because this proposed method cannot be effectively removes the noise and staircase artifacts.
16.	Restoration of Poisson noise corrupted digital images with nonlinear PDE based filters along with the choice of regularization parameter estimation (Rajeev et. al. 2013)	In this paper, the reconstruction of three nonlinear partial differential Eq.s (PDE) based filters adapted to Poisson noise statistics have been proposed in a variational framework for restoration and enhancement of digital images corrupted with Poisson noise. The proposed and examined PDE based filters include total variation adapted to Poisson noise in L-1 framework; anisotropic diffu-	The comparative analysis of the proposed methods are presented in terms of relative norm error, improvement in SNR, MSE, PSNR, CP and MSSIM for an adaptive value of regularization parameter calculated by every methods in consideration. Finally the obtained results it is ob-	Future work will be devoted for extending the model to handle the 3D and color denoising cases.

		sion; and complex diffusion based methods adapted to Poisson noise in L-2 framework.	served that the anisotropic diffusion based method adapted to Poisson noise gives better results in comparison to other methods in consideration along with choice of GCV for regularization parameter selection.	
17.	Application of regularized maximum likelihood algorithm in PET image reconstruction combined with nonlocal fuzzy anisotropic diffusion (Quan Zhanga *et.al.* 2013)	Author propose a novel regularized maximum likelihood reconstruction algorithm for PET imaging, which uses the fuzzy nonlinear anisotropic diffusion as the regularization to reduce noise and preserve edges.	The proposed algorithm not only absorbs the advantages of fuzzy set theory in deal with uncertain problems, but also has the good ability of anisotropic diffusion, namely protecting edges perfectly and suppressing noise.	The noise effect and staircase artifacts, image intensity will still be not observed in the corresponding reconstructed image by using the proposed method.
18.	Penalized Maximum Likelihood Algorithm for Positron Emission Tomography by Using Anisotropic Median-Diffusion (Qian He, 2014)	In this paper, a novel penalized maximum likelihood (PML) algorithm is presented for improving the quality of PET images. The proposed algorithm fuses an anisotropic median diffusion (AMD) filter to the maximum-likelihood expectation-maximization (MLEM) algo-	The fusing algorithm shows its positive effect on image reconstruction and denoising. Experimental results present that the proposed method denoises and reconstructs images with high quality.	The proposed method still suffer from stair casing effects and used manual value the diffusion coefficient (k) and other controlling AD param-

		rithm.		eters.
19.	Alternating Direction Method of Multiplier for Tomography With Nonlocal Regularizer (Se Young Chun et.al. 2014)	This paper use variable splitting to separate the likelihood term and the regularizer term for penalized emission tomographic image reconstruction problem and to optimize it using the alternating direction method of multiplier (ADMM). We also propose a fast algorithm to optimize the ADMM parameter based on convergence rate analysis.	ADMM improved the speed of convergence substantially compared to other existing methods such as gradient descent, EM, and OSEM using De Pierro's approach, and the limited-memory Broyden–Fletcher–Goldfarb – Shanno algorithm.	Improving image quality with proper regularizer and appropriate regularization parameter selection using this fast ADMM algorithm will be an important and interesting future work.
20.	Nonlocal means-based regularizations for statistical CT reconstruction (Hao Zhang *et. al.*, 2014)	Inspired by the success of nonlocal means (NLM) algorithm in image processing applications, author proposed, a family of generic and edge preserving NLM-based regularizations for SIR.	SIR with the proposed regularization can achieve more significant gains than SIR with the widely-used Gaussian MRF regularization and the conventional FBP method, in terms of image noise reduction and resolution preservation.	Further works is needed to improve the visual quality for real clinical images because this proposed method cannot be effectively removes the noise and staircase artifacts.
21.	Iterative image reconstruction for limited-angle inverse helical cone-beam computed tomography	In this work, a fast iterative reconstruction algorithm based on total variation minimization is developed for a trajectory of limited-angle inverse helical cone-beam CT, which can be applied to	The experimental results show that the developed algorithm can yield reconstructed images of low noise level and high image quality.	The algorithm developed is mainly focus on limited-angle inverse helical cone-beam CT, it doesn't pro-

	(Wei Yu *et. al.,* 2015)	detect long-object without slip-ring technology.		vide solution to other imaging mode including low dose or few-view CT imaging and half covered CT imaging and so on.
22.	NUFFT-Based Iterative Image Reconstruction via Alternating Direction Total Variation Minimization for Sparse-View CT (Bin Yan *et. al.* 2015*)*	A novel Fourier-based iterative reconstruction technique that utilizes non-uniform fast Fourier transform is presented in this study along with the advanced total variation (TV) regularization for sparse-view CT.	The proposed method has higher computational efficiency and better reconstruction quality than the conventional algorithms, such as SART using TV method and the alternating direction TV minimization approach, with the same time duration.	Proposed NUFFT cannot effectively solve the problems in sparse-view image reconstruction. The NUFFT just was especially applied as a transition during iteration in spatial domain, which in turn burdened computation consumption.

The Statistical iterative reconstruction (SIR) (F. Benvenuto *et. al.,* 2008; Quan Zhang *et. al.,* 2013; R. Vijayarajan et al., 2014) methods are needed for low-dose CT imaging, where measured data is an essential factor to be considered in the image reconstruction (similar to the count-limited imaging modalities of single photon emission computed tomography (SPECT) and positron emission to-

mography (PET)), Essentially, the SIR methods search for the image or solution that makes the projection measurements the most probable. Instead of treating all the measurements equally, a statistical model provides different degrees of credibility/reliability among measurements according to the signal-to-noise ratio (Thibault et al 2007). Table 2.3 illustrates brief survey on recent methodology used in statistical image reconstruction methods for low dose X-ray CT.

Table 2.3: Recent Methodologies used in Low-Dose X-ray CT

S.No.	PAPERS	BRIEF DESCRIPTION	ADVANTAGES	LIMITATIONS
1.	Low Dose CT Reconstruction via Edge-preserving Total Variation Regularization (Tian et al-2011)	The edge preserving TV term is proposed to preferentially perform smoothing only on non-edge part of the image in order to better preserve the edges, which is realized by introducing a penalty weight to the original total variation norm.	During the reconstruction process, the pixels at edges would be gradually identified and given small penalty weight.	GPU is employed but still speed of this iterative method cannot compete with speed of conventional FBP. Efficiency of algorithm should be improved.
2.	Bayesian sinogram smoothing with an anisotropic diffusion weighted prior for low-dose X-ray computed tomography. *(Zhang et al-2012)*	This method presents a novel anisotropic diffusion weighted prior applied in Bayesian-based statistical sinogram smoothing approach.	The reconstructed image is more uniform at the flat region while preserving the matched resolution with the GS-PRWLS result, especially in the region of interest and Thus, the proposed method outperforms the GS-PRWLS.	Further investigation is required for the measures setting the smoothing parameter *t* adaptively and the proposed approach is not applicable to three dimensions cone-beam CT.
3.	Penalized likeli-	This paper presents a patch-	The new regularization is	High computa-

	hood PET image reconstruction using patch-based edge preserving regularization (Wang and Qi, 2012)	based regularization for IR methods that uses neighborhood patches instead of individual pixels in computing the non-quadratic penalty.	more robust than the conventional pixel-based regularization in differentiating sharp edges from random fluctuations due to noise.	tion load and complex mathematical model. The full benefit of this proposed algorithm for real PET studies will be evaluated in future.
4.	Adaptive weighted total variation minimization for sparse data toward low-dose x-ray computed tomography image reconstruction (Liu, 2012)	The AwTV model is derived by considering the anisotropic edge property among neighboring image voxels, where the associated weights are expressed as an exponential function and can be adaptively adjusted by the local image-intensity gradient for the purpose of preserving the edge details.	The results show that the presented AwTV-POCS algorithm can yield images with several notable gains, in terms of noise-resolution tradeoff plots and full-width at half-maximum values, as compared to the corresponding conventional TV-POCS algorithm.	Convergence speed similar to the previously compared model TV-POCS. Further it needs different data constraints with associated optimization strategies for different applications. Only applicable for large clinical data.
5.	The adaptive sinogram restoration algorithm based on anisotropic diffusion by energy minimization for low-dose X-ray CT. (Cui et. al., 2013)	This method proposes a novel sinogram noise reduction method by energy minimization. An adaptive smoothness parameter based on a modified anisotropic diffusion coefficient is applied for an optimal estimation.	The proposed smoothing method has much higher Signal to Noise Ratio (SNR) value than that of GS-PRWLS and MADF reconstructed image.	Gradient (of sinogram data) is sensitive to the noise and is liable to bring error in the edge detection.

6.	Statistical image reconstruction for low-dose CT using nonlocal means-based regularization. (Zhang et. al., 2014)	Inspired by the success of nonlocal means (NLM) in image processing applications, in this work, we propose to explore the NLM-based regularization for SIR to reconstruct low-dose CT images from low-mAs acquisitions.	Both digital and physical phantoms consistently demonstrated that SIR-NLM-based regularization can achieve more gains than SIR with the well-known Gaussian MRF regularization or the generalized Gaussian MRF regularization and the conventional FBP method, in terms of image noise reduction and resolution preservation.	Major drawback of the iterative proposed methods is their computational burden due to the multiple re-projection and back-projection operation cycles in the projection and image domains.
7.	Statistical image reconstruction for low-dose CT using nonlocal means-based regularization. Part II: An adaptive approach (Zhang, 2014f)	From our previous investigation on NLM-based strategy, we noted that using a spatially invariant filtering parameter in the regularization was rarely optimal for the entire field of view (FOV). Therefore, in this study we developed a novel strategy for designing spatially variant filtering parameters which are adaptive to the local characteristics of the image to be reconstructed.	The necessity in introducing the spatial adaptively and the efficacy of the adaptively in achieving superiority in reconstructing CT images from low-dose acquisitions.	The first one is the parameters tuning. While the sizes of search-window and patch-window (also the standard deviation of the Gaussian kernel) do not show noticeable effects on the reconstructed image.
8.	Iterative Reconstruction for X-Ray Computed Tomography us-	In this study, propose a prior-image induced nonlocal (PINL) regularization for statistical iterative reconstruc-	Specifically, the PINL regularization utilizes the redundant information in the prior image and the	Major drawback of the present PWLS-PINL algorithm is that

	ing Prior-Image Induced Nonlocal Regularization (Zhang, 2014c)	tion via the penalized weighted least-squares (PWLS) criteria, which we refer to as "PWLS-PINL".	weighted least-squares term considers data-dependent variance estimation, aiming to improve current low-dose image quality.	the update of the nonlocal weights matrix unavoidably increases the computational burden
9.	Sparse-view x-ray CT reconstruction via total generalized variation regularization. (Niu *et. al.*, 2014)	To eliminate the undesired patchy artifacts from the TV-based methods, a total generalized variation (TGV) regularization is adapted under the penalized weighted least-squares (PWLS) criteria for CT image reconstruction from sparse view projection measurements	The resolution property of the presented PWLS-TGV method was studied using a modulation transfer function (MTF), which characterizes the spatial resolution of images. Also, we can observe that the PWLS-TGV method can yield a better image resolution than the PWLS-TV method in 30, 40 and 60 view projections.	Optimization approach in this method is separable paraboloidal surrogates algorithm is used. Therefore convergence rate is very slow in this method.
10.	Median prior constrained TV algorithm for sparse view low-dose CT reconstruction. (Liu *et. al.*, 2015)	First, an auxiliary vector m in register with the objective function of TV is introduced, so that the target pixel was close to its local median in each iteration process. Next, the obtained results were also analyzed in detail in order to verify the effectiveness of this new algorithm	The SNR values of TV_MP reconstructions are still need to improve than other results, nether neither the results of TV nor those of TV reconstruction + 2D median filter.	This proposed method is limited to parallel-beam CT and it is not for Cone-beam or fan-beam and real CT systems.

2.5. Noise model

Images are often suffered by noise during acquisition and transmission, which degrades the quality of the images. During image reconstruction, the noise contained in the data measured by imaging instruments is primarily poisson type and decreasing the noise has the potential to optimize the quality of CT and PET images. In this section, we discuss the statistical properties of three common types of noise found in CT/PET medical image reconstruction process (Poisson, Gaussian, and mixed type (Gaussian +Poisson)) and show the relationship for each of them.

2.5.1. Poisson noise model

A Poisson data-noise model arises in many inverse problems applications. In medical image processing, in particular, a charge-coupled-device (CCD) camera is often used to measures image intensity via the counting of incident photons. Counting processes are known to have error that is well-modeled by a Poisson distribution. Therefore, a standard Poisson data-noise model as described in (D. L. Snyder, 1993) is presented, and the measurements follow independent Poisson random distribution is as follows:

$$y_i \propto Poisson\left(\bar{y}_i(f)\right), \quad i=1,....,I \tag{2.32}$$

where y_i is the measured projectional data which are counted by the i^{th} detector with expectation $\bar{y}_i$ as a function of the underlying attenuation map for PET/SPECT or transmission tomography during the data collection, f represents the estimated image vector and the element of f denotes the activity of image. In iterative methods, the calculation of the system matrix during the reconstruction process is essential and given as follows:

$$\bar{y}_i(f)=\sum_{j}^{J} a_{ij} f_j \tag{2.33}$$

where a_{ij} is the system matrix or geometric probability that an emission from image pixel j is detected by the detector i in ideal conditions, which describes

the relationship between the measured projection data and the estimated image vector. The probability distribution function (pdf) of the Poisson noise reads:

$$P(y|f)=\prod_{i}^{I}\frac{\bar{y}_i(f)^{y_i}}{y_i!}\exp\left(-\bar{y}_i(f)\right), \tag{2.34}$$

and the corresponding log-likelihood can be described as follow:

$$L(f)=\log P(y|f)=\sum_{i=1}^{I}\left(y_i\log\left(\sum_{j=1}^{J}a_{ij}f_j\right)-\sum_{j=1}^{J}a_{ij}f_j\right) \tag{2.35}$$

where I is the number of detector pairs, J is the number of the objective image pixels, and $P(y|f)$ is the probability of the detected measurement vector y with image intensity f. According to maximum a posterior (MAP) estimator, the reconstructed image can be obtained by maximizing the log-likelihood function $L(f)$, i.e.,

$$L(f)=\arg\max_{f\geq 0}L(f) \tag{2.36}$$

To solve the optimization problem of iterative methods given by Eq. (2.36), Shepp and Vardi [14] proposed the MLEM algorithm, and the iterative formula can be described as follows:

$$f_j^{k+1}=\frac{f_j^k}{\sum_{i=1}^{I}a_{ij}}\sum_{i=1}^{I}\frac{a_{ij}y_i}{\sum_{l=1}^{J}a_{il}f_l^k} \qquad \textit{for } j = 1, 2,. . . . , N. \tag{2.37}$$

2.5.2. Gaussian noise model

This most common type of noise results from the contributions of many independent signals. This is a consequence of the central limit theorem which states that the sum of many random variables with various PDFs results in a signal with a Gaussian PDF. Noise modelling of the projection (or sinogram) data, specifically for low-dose CT, is essential for the statistics-based image restoration algorithms. Previous studies have indicated that the calibrated and log-transformed projection data of low-mA CT protocols are assumed to follow approximately a Gaussian distribution, with an associated relationship between the

data sample mean and variance. Let the formation of X-ray CT images can be modeled approximately by a discrete linear system as follows:

$$y = Af, \tag{2.38}$$

where $f = (f_1, f_2, ..., f_N)^T$, is the original image vector to be reconstructed, N is the number of voxels, the superscript T is the transpose operator, $y = (y_1, y_2, ..., y_M)^T$, is the measured projection vector data, M is the total number of sampling points in the projection data, $A = \{a_{ij}\}, i = 1, 2, ...M \text{ and } j = 1, 2, ..., N.$ is the system matrix, relating f and y, with the size $I \times J$, and its element a_{ij} is typically calculated as the inter-section length of projection ray i with pixel j.

The line integral along an attenuation path is calculated according to the Lambert–Beer's law:

$$\tilde{y}_i = \ln\left(\frac{N_{0i}}{\tilde{N}_i}\right), \quad y_i \simeq \ln\left(\frac{N_{0i}}{N_i}\right) \tag{2.39}$$

where N_{0i} represents the mean number of X-ray photons just before entering the patient and going toward the detector bin i, and can be measured by system calibration, e.g., by air scans; N_i denotes the detected photon counts at detector bin i with expected value $\tilde{N}_i$. The approximation for the second Eq. in (2.39) reflects an assumption that the Lambert–Beer's law can be applied to the random values (Zhang H *et. al.,* 2014). The Gaussian distribution for X-ray CT can be described by the following analytical formula (Zhang H *et. al.,* 2014; Whiting Bruce *et. al.,* 2014):

$$\sigma_i^2 = f_i \times \exp\left(\frac{x_i}{\eta}\right), \tag{2.40}$$

where x_i is the mean and σ_i^2 is the variance of the projection data at detector channel or bin i, and both η and f_i are object-independent parameters, which are completely determined by the system or manufacture configuration. Notation f_i is a parameter adaptive to detector channel i which can be computed from the repeated projections.

Image reconstruction problem is naturally represented in terms of energy minimization. In this framework, the data energy comes from the (negative) log likelihood function of the observed projection data (Liu Li *et. al.,* 2012). From Eq.(2.40), we see that the calibrated and log transformed projection data of low-mA CT protocol follow approximately a Gaussian distribution with mean and variance , after the *isolated datum* removal. In addition, it can be assumed that the observation at each pixel is nearly independent from other observations (Niu Shanzhou *et. al.,* 2014). Hence the conditional probability of the observed calibrated sinogram given the sinogram image can be simply expressed as:

$$f_{(y|x)} = \prod_{i=1}^{M} f\left(y_i \middle| x_i\right) = \prod_{i=1}^{M} \frac{1}{\sqrt{2\pi\sigma_i^2}} \exp\left(-\frac{\left(y_i - x_i\right)^2}{2\sigma_i^2}\right), \quad (2.41)$$

Based on the previous studies, (Yu, Lifeng *et. al.,* 2015; Zhang H *et. al.,* 2014; Gao Yang *et. al.,* 2014; Zhang *et. al.,* 2010; Liu Li *et. al.,* 2012; Cui Xueying *et. al.,* 2014; Jing Wang *et. al.,* 2008; Liu Yan et. al., 2012; Lui Dorothy et. al., 2013) found that two principal sources of CT transmission data noise, X-ray quanta noise (signal–dependent compound Poisson distribution) and system electronic background noise (signal–independent Gaussian or normal distribution with zero mean). However, it is numerically difficult to directly implement these models for data noise simulation. Several reports have been discussed approximation of this model by the Poisson model (Liu Li *et. al.*, 2012).

2.5.3. Gaussian-Poisson noise model

Practically, the measured transmission data can be assumed to statistically follow the Poisson distribution upon a Gaussian distributed electronic background noise (Ghita, O et. al., 2010):

$$N_i \approx Poisson\left(\tilde{N}_i\right) + Gaussian\left(m_e, \sigma_e^2\right) \quad (2.42)$$

where m_e and σ_e^2 are the mean and variance of the Gaussian distribution from the electronic background noise, $\tilde{N}_i$ is the mean of Poisson distribution.. In reality, the mean m_e of the electronic noise is often calibrated to be zero (i.e., 'dark cur-

rent correction') and the associative variance slightly changes due to different settings of tube current, voltage and durations in a same CT scanner (F. Benvenuto, 2008). Hence, in a single scan, the variance of electronic background noise can be considered as uniform distribution. Based on the noise model (2.38) and the use of the Lambert-Beer's law (2.39), the calibrated and log-transformed projection data follow approximately a Gaussian distribution with an associated relationship between the data sample mean and variance, which can be described by the following analytical formula (Phillippe P. Bruyant, 2002):

$$\sigma_i^2 = \frac{1}{N_{0i}} \exp\left(\tilde{y}_i\right)\left(1+\frac{1}{N_{0i}} \exp\left(\tilde{y}_i\right)\left(\sigma_e^2 - 1.25\right)\right) \tag{2.43}$$

where N_{0i} is the incident x-ray intensity, $\tilde{y}_i$ is the mean of the log transformed ideal sinogram datum y_i along path *i*, and σ_e^2 is the background Gaussian noise variance. In the implementation, the sample mean $\tilde{y}_i$ could be estimated by neighborhood averaging with a 3×3 window. The parameters N_{0i} and σ_e^2 can be measured as part of the standard routine calibration operation in modern CT systems (Gao Yang *et. al.*, 2014).

According to previous studies (Yu, Lifeng *et. al.*, 2015; Zhang H *et. al.*, 2014; Gao Yang *et. al.*, 2014; Zhang *et. al.*, 2010; Liu Li *et. al.*, 2012; Cui Xueying *et. al.*, 2014; Jing Wang *et. al.*, 2008; Liu Yan et. al., 2012; Lui Dorothy et. al., 2013), the noisy line integral along an attenuated measurements can be treated as normally distributed with a non-linear signal-dependent variance (Liu Yan et. al., 2012; Lui Dorothy et. al., 2013). Assuming that the measurements among different bins are statistically independent, the likelihood function of the joint probability distribution, given a distribution of the attenuation coefficients, can be written as:

$$P\left(y \middle| f\right) = \frac{1}{Z_0} \prod_i \exp\left[-\frac{\left(y_i - f_i\right)^2}{2\sigma_i^2}\right] \tag{2.44}$$

where Z_0 is a normalizing constant, $y = \left(y_1, y_2, ..., y_M\right)^T$, is the is the measured projection vector data.

Then, ignoring the constant and irrelevant terms, and by taking the negative log-likelihood function can be written as:

$$L(y|f) = \ln P(y|f) = \sum_{i=1}^{M} \left\{ \frac{(y_i - f_i)^2}{2\sigma_i^2} \right\} \tag{2.45}$$

Due to the presence of an extremely limited number of X-ray projections, noise and other inconsistencies in the acquired sinogram data of CT image reconstruction causes an ill-posedness problem (Chen Y.*et. al.,* 2010). Therefore, the image estimation that directly optimizes the Maximum Likelihood (ML) criterion can be very noisy and unstable. So researchers reformulate this problem with the MAP estimation by posing a prior term to penalize or regularize the solution. The prior term enables us to incorporate available information or expected properties of the image to be reconstructed.

2.6. Maximum a posteriori (MAP) estimation

Mathematically, CT and PET image reconstruction is an ill-posed problem due to the presence of noise and other inconsistencies in the projection data. Therefore, the image estimation that directly optimizes the ML criterion can be very noisy and unstable. So the above mentioned problem can be reformulated with the MAP estimation by posing a prior term to penalize or regularize the solution. The prior term enables us to incorporate available information or expected properties of the image to be reconstructed. Mathematically, the MAP estimator can be expressed as (Green, 1990):

$$f^* = \arg\max_f P(f|y) \tag{2.46}$$

According to the Bayesian law:

$$P(f|y) = \frac{P(y|f)P(f)}{P(y)} \tag{2.47}$$

By taking the logarithm and omitting the irrelevant term the MAP estimator can be simplified to:

$$f^* = \arg\max_f \left[\ln P(f|y) \right] = \arg\max_f \left[L(y|f) - R(f) \right] = \arg\max_f \left[L(y|f) - \lambda U(f) \right] \quad (2.48)$$

where *U(f)* denotes a penalty, and $\lambda > 0$ is a scalar control parameter which allows one to tune the MAP (or penalized ML (pML)) estimation for a specific noise-resolution tradeoff. When the value of λ goes to zero the reconstructed image from the MAP estimation approach behaves like the ML estimation.

The SIR of low-dose CT can be considered to estimate the attenuation map by maximizing the MAP (or pML) criterion with a non-negativity constraint (using the calibrated transmitted photon counts):

$$f^* = \arg\max_{f \geq 0} \left[L(y|f) - \lambda U(f) \right] \quad (2.49)$$

or directly minimizing the objective function by variational framework (using the calibrated line-integrals):

$$f^* = \arg\min_{f \geq 0} \left[\sum_{i=1}^{M} \frac{(y_i - f_i)^2}{2\sigma_i^2} + \lambda U(f) \right] \quad (2.50)$$

where $U(f)$ denotes the regularization term(e.g., the log-prior) and λ is the smoothing parameter that controls the trade-off between the data-fidelity term(e.g., the log-likelihood) and regularization term . In next section, we present the various possible choices available in literature for the regularization function or prior or penalty function $U(f)$.

2.7. Regularization

The use of prior information can greatly improve the reconstruction quality, especially when the observed data are incomplete or corrupted by noise. In this section, the importance of regularization strategies explicitly used in various statistical image reconstruction (SIR) algorithms is presented. The regularization term incorporates prior knowledge or expectations of smoothness or other characteristics in the image, which can help to stabilize the solution and suppress the noise and streak artifacts. Under the Bayesian framework, the regularization

functional *U* needs to reflect our *a priori* knowledge on the unknown function *f*, primarily in term of its *smoothness*. There exist also non Bayesian methods for the regularization of inverse problems, where the prior information is not expressed as probability distribution.Various regularizations have been presented in the past decades based on different assumptions, models and knowledge. Although some of them were initially proposed for SIR of SPECT and PET, they can be readily employed for CT. The statistical modelling of the projection measurements is a prerequisite for building the data-fidelity term, and the regularization term also has a strong influence on the quality of reconstructed images. In clinical CT systems, the raw signals from detectors are always pre-processed by CT vendors for various degrading factors such as scattered radiation, beam hardening, detector non-uniformity and so on (Hsieh 2009), while the raw signals (considered proprietary by vendors) are rarely accessible to academic researchers. Therefore, the researchers generally focus on investigating the properties of pre-processed CT signals in the past decades (Lu et al 2001; Whiting 2002; Li et al 2004; Whiting et al 2006; Wang et al 2008b; Ma et al 2012a). Commonly, the accessible projection data are calibrated transmitted photon counts (before log-transform) or calibrated line integrals (after log-transform). With the monochromatic X-ray assumption, the statistics of calibrated transmitted photon counts can be described by a Poisson distribution (Macovski 1983) or 'Poisson+Gaussian' distribution with consideration of additional electronic noise (Snyder et al 1993; Snyder et al 1995). This assumption has been well accepted in the CT field under the observations that although the polychromatic X-ray quanta may follow a Compound Poisson distribution (Whiting 2002; Elbakri and Fessler 2003; Whiting et al 2006), the difference from the Poisson distribution is small and merely on the variance (Li et al 2004). Meanwhile, the noise properties of calibrated line integrals have also been validated by experimental studies of repeated scans, and the statistical analysis showed that calibrated line integrals can be fitted approximately by a Gaussian distribution with a nonlinear signal-dependent variance (Lu et al 2001; Li et al 2004; Wang et al 2008b), regardless of the consideration of electronic noise (Ma et al 2012a). Therefore, existing SIR methods for X-ray CT either use calibrated transmitted photon counts with a simple Poisson approximation (or 'Poisson +Gaussian' approximation) or calibrated line integrals with a Gaussian approximation.

Based on Markov random fields (MRF) theory (Srivastava Subodh et. al., 2012), the original ill-posed reconstruction can be greatly improved by Bayesian methods (Feng QJ., 2006). How to devise an effective prior for Bayesian reconstruction has been widely studied in the past 10 years (Yang Chen, 2007). Lowering the noise effect and preserving the edges are the two main aims in devising priors. But one drawback of these priors is their tendency to uniformly penalize the image or the image gradient irrespective of the underlying image structures and the difference of signal-dependent noise properties in different regions. As a result, edges are sometimes over smoothed, leading to loss of detailed information. To address this drawback, several edge-preserving regularization terms were proposed in the literature (Rudin et al 1992, Yu and Fessler 2002, Ma et al 2010, Ma et al 2012a, Liu et al 2012, Liu et al 2014). A typical example is total variation (TV) regularization with the piecewise constant assumption (PCA) (Rudin et al 1992, Panin et al 1999). Extensive studies have shown that high-quality CT image can be reconstructed via TV minimization from sparse-view measurement without introducing noticeable artifacts (Liu et al 2014, Niu and Zhu 2012, Park et al 2012, Sidky et al 2006). However, PCA often leads to the appearance of noticeable patchy artifacts in reconstructed images (Tang et al 2009, Bian et al 2010, Liu et al 2012). The simple and widely used quadratic membrane (QM) prior tends to produce an unfavorable over smoothing effect. And some edge-preserving non-quadratic priors are able to produce sharp edges by choosing a non-quadratic prior energy [8–13]. And in 1998, edge-preserving median root prior (MRP) was proposed by Alenius and his colleagues for iterative reconstruction of PET transmission images [11]. However, in the case of low X-ray scan when the noise level is relatively significant, such edge-preserving non-quadratic priors tend to produce blocky piecewise regions or staircase artifacts. None of these priors addresses the information of global connectivity and continuity in objective image. Only local and in discriminatively prior information is provided. We term these traditional priors local priors. Yu and Fessler devised a boundary-based Bayesian method which incorporates global information of image by level-set methods (Hongchuan yu, 2004). But such boundary-based method relies heavily on the level-set operations whose effect in different images is unpredictable and parameter-dependent. Recently, Buades et al. put forward a novel algorithm for

image denoising (Yuanquan Wang, 2008). Illuminated by their nonlocal idea, a nonlocal MRF quadratic prior model for Bayesian image reconstruction is proposed (Chen Y *et. al.*, 2010; Zhen Tian *et. al.*, 2011). Rest of the section presents the detailed description about the various performance measures and data sets used in this thesis for quantitative and qualitative analysis purposes.

2.8. Performance Measures

The EM algorithm is an iterative method. Stopping the algorithm at certain iteration where the image quality is supposed to be optimum, offers a solution to the problem of image deterioration. The main difficulty of defining a stopping rule is that in the EM, the likelihood function is monotonically increasing and does not provide any direct information on the quality of the reconstructed image in terms of noise and edge artefacts. Therefore the asymptotic curve of likelihood function is not of practical interest because as the likelihood value increases, noise and edge artefacts are increasing too.

In this section of the work, results and performance analysis of the proposed method are presented for three different computer generated CT/PET/SPECT phantoms and one standard medical thorax image both qualitatively and quantitatively. In this simulation study, only two- dimensional (2-D) simulated phantoms were considered. This was because our main aim here is to compare proposed hybrid method with other algorithms and to demonstrate that the proposed method was applicable to different imaging modalities such as CT/PET/SPECT, where 2-D phantoms were sufficient for this purpose. For simulation study MATLAB 2013b software was used on PC with Intel(R) Core (TM) 2 Duo CPU U9600 @ 1.6GHz, 4.00 GB RAM, and 64 bit Operating system. For quantitative analysis the various performance measures used include signal-to-noise ratio (SNR), the root mean square error (RMSE), the peak signal-to-noise ratio (PSNR), the correlation parameter (CP) (Rajeev *et. al.*, 2011), and mean structure similarity index map (MSSIM) (Rajeev *et. al.*, 2011). The SNR, RMSE and PSNR give the error measures in reconstruction process. The correlation parameter is a measure of edge preservation in the reconstructed im-

age. The MSSIM is a measure of preservation of luminance, contrast and structure of the image after the reconstruction process, which is necessary for medical images. The brief definitions of these quantitative measures are given as follows:

- **Signal-to-Noise-Ratio (SNR) is defined as** (Rajeev *et. al.*, 2011)**:**

$$SNR\%\left(f_{REC},f_{ORIG}\right)=10\log 10\frac{\sum_{x=1}^{M}\sum_{y=1}^{N}\left[f_{REC}(x,y)-\bar{f}\right]^2}{\sum_{x=1}^{M}\sum_{y=1}^{N}\left[f_{REC}(x,y)-f_{ORIG}(x,y)\right]^2}\times 100\%, \quad (2.51)$$

where, the numerator and denominator stand for the signal power and the noise power, respectively. f_{REC}, $\bar{f}$ and f_{ORIG} denote the reconstructed image, the average gray scale of all pixels in reconstructed image, and the corresponding original numerical phantom image, respectively. A bigger SNR value indicates a better performance of the corresponding reconstruction result.

- **Root Mean Square Error (RMSE):** This item measures how the reconstructed image is close to the phantom image i.e.

$$RMSE\%\left(f_{REC},f_{ORIG}\right)=\sqrt{\frac{\sum_{x=1}^{M}\sum_{y=1}^{N}\left[\hat{f}_{j\,REC}(x,y)-f^{*}_{j\,ORIG}(x,y)\right]^2}{J^2}}\times 100\%, \quad (2.52)$$

where, notation $f_{REC}(x,y)$ and notation $f_{ORIG}(x,y)$ denote the value of pixel j of the reconstructed image and that of the original image, respectively. J is the number of pixels of the image. The best algorithm will give the minimum value of root mean square error.

- **Peak signal-to-noise ratio (PSNR)** (Rajeev *et. al.*, 2011)**:**

$$PSNR\%\left(f_{\mathrm{R}EC},f_{ORIG}\right)=10\log_{10}\left[\frac{255\times 255}{RMSE}\right]\times 100\% \quad (2.53)$$

Here, RMSE is the root mean square error which is defined above. For optimal performance, measured values of RMSE should be small and that of PSNR should be large.

- **The structural Similarity (SSIM) index** (Rajeev *et. al.*, 2011) measures the similarity between two images given one image has perfect quality. SSIM was used on the synthetic noise compensated image to measure the similarity between the ground truth and the corrected image based on three comparisons: luminance, contrast and structure. **The mean SSIM (MSSIM)** can be measured using the following formulation for the original image $f_{ORIG}(x,y)$ and the reconstructed image $f_{REC}(x,y)$:

$$MSSIM\%\left(f_{REC,}f_{ORIG}\right)=\frac{1}{M}\sum_{j=1}^{M}SSIM\left(x_j,y_j\right)\times 100\% \tag{2.54}$$

$$SSIM(x,y)=\frac{\left(2\mu_x\mu_y+C_1\right)\left(2\sigma_{xy}+C_2\right)}{\left(\mu_x^2+\mu_y^2+C_1\right)\left(\sigma_x^2+\sigma_y^2+C_2\right)} \tag{2.55}$$

The parameters C_1 and C_2 are constants that avoid instability when the local means *x* and *y* and local standard deviations σ_x and σ_y are close to zero. An MSSIM measure equal to 1 indicates perfect similarity with the original image. The definitions of **correlation parameter (CP):**

- **Correlation parameter (CP)** (Rajeev *et. al.*, 2011)**:**

Correlation parameter (CP) is a qualitative measure for edge preservation. If one is interested in suppressing speckle noise while at the same time preserving the edges of the original image then this parameter proposed by (Rajeev *et. al.*, 2010) can be used. To evaluate the performance of the edge preservation or sharpness, the correlation parameter is defined as follows (Rajeev *et. al.*, 2011):

$$CP\%\left(f_{REC,}f_{ORIG}\right)=\frac{\sum_{i=1}^{m}\sum_{j=1}^{n}(f_{ORIG_j}(x,y)-\bar{f}_{ORIG_j})\times(f_{REC_j}(x,y)-\bar{f}_{REC_j})}{\left[\sum_{i=1}^{m}\sum_{j=1}^{n}(f_{ORIG_j}(x,y)-\bar{f}_{ORIG_j})^2\times\sum_{i=1}^{m}\sum_{j=1}^{n}(f_{REC_j}(x,y)-\bar{f}_{REC_j})^2\right]^{\frac{1}{2}}}\times 100\% \tag{2.56}$$

where $f_{ORIG_j}(x,y)$ and $f_{REC_j}(x,y)$ refers to the value of pixel *j* of the original image and that of the reconstructed image respectively, $\bar{f}_{ORIG_j}$ and $\bar{f}_{REC_j}$ repre-

sents the image average value in the original images and reconstructed images respectively via a 3x3 pixel standard approximation of the Laplacian operator. The correlation parameter should be closer to unity for an optimal effect of edge preservation.

2.9. Dataset Description

The brief description of the three computer generated phantoms and one standard medical thorax phantom image are given as follows: Fig. 2.9, shows the visuals of the test phantoms used for the simulation purposes. These test phantoms are (a) Modified Shepp-Logan phantom (128×128 pixels), (b) PET Test phantom (128×128 pixels), (c) SPECT Test phantom (128×128 pixels), (d) Medical thorax image (128×128 pixels).

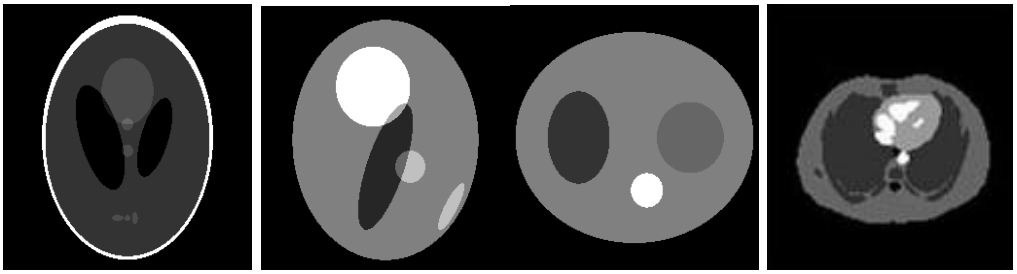

Fig. 2.9: The phantoms used in the simulation study, (a) Modified Shepp-Logan phantom (128×128 pixels), (b) PET Test phantom (128×128 pixels), (c) SPECT Test phantom (128×128 pixels), (d) Medical thorax image (128×128 pixels).

Test case 1:

For Test case 1, the modified Shepp-Logan phantom with 128×128 pixels was used. There were 90 projections uniformly spaced over 360° angles and each projection contained 150 measurements (thus n = 13500). The system matrix p_{ij} (with dimensions 13500×4096 was determined by the geometry of the pixels. Poisson noise was added to the expected projections $G = Px$ to form the observed measurement vector *y*. To generate Poisson noise, the *poissrnd* and *randn* function in MATLAB's statistical Toolbox was used. The total projection count was 6×10^5. For simulation study of the proposed method with this phantom various parameters and iteration cycles were tried to get the best performance. Figure 2.10 show the visuals of the phantom which consists of different

size of ellipses with differing intensity aiming to test the performance of the various standard and proposed reconstruction algorithms.

Fig. 2.10: Modified Shepp-Logan phantom (128×128 pixels)

Test case 2:

Test case 2 is a computer generated mathematical PET test phantom is shown in Fig. 2.11, which made up of five ellipses and is chosen as a simplified imitation of the brain's metabolic activity. To generate Poisson noise, the *poissrnd* and *randn* function in MATLAB's statistical Toolbox was used. The total projection count was 6×10^5. The other test case generation parameters are similar to test case 1.

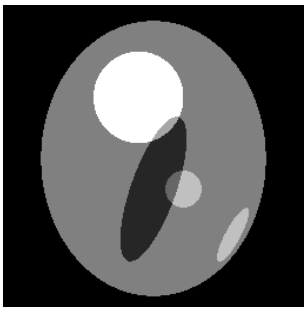

Fig. 2.11: PET Test phantom (128×128 pixels),

Test case 3:

For the test case 3, the simulation generated projection data using the activity map (or "phantom") is shown in Fig. 2.12. This elliptical phantom of axes dimensions are 64 cm 51.2 cm and 16 cm represents a chest area cross section of a human body: the circles represent the low and high activity of the lungs corresponds to the myocardium. Projection was consistent with SPECT geometry. We simulated 64 attenuated parallel beam projections, with projections uniformly spaced over360°, each comprising 64 attenuated projection measurements.

The simulation was conducted using MATLAB. The projection matrix (with dimension) was calculated using the geometry of pixels and projections and attenuation as above. The expected projection vector was generated by matrix-vector multiplications based on the sparse projection matrix and the digitized image vector, fixing a total expected projection count of 400000. This procedure introduces small discretization errors associated with setting uniform activity within pixels in projection. The observed projection data were then generated from with Poisson noise. The total observed count was 400605.

Fig.2.12: SPECT Test phantom (128×128 pixels)

Test case 4

Fig. 2.14 shows the fourth test image which is the standard thorax medical image. Projections are calculated mathematically. The original test image is gray-scale image of size 128×128, with coverage angle ranging from 0° to 360° with rotational increment of 0° to 10°.

Fig.2.13: Medical thorax image (128×128 pixels)